Mon. Not. R. Astron. Soc. **394,** 21–37 (2009) doi:10.1111/j.1365-2966.2008.14042.x

SN 1994W: an interacting supernova or two interacting shells?

Luc Dessart,[1,2]★ D. John Hillier,[3] Suvi Gezari,[4] Stéphane Basa[5] and Tom Matheson[6]

[1]*Department of Astronomy and Steward Observatory, The University of Arizona, Tucson, AZ 85721, USA*
[2]*Department of Astrophysical Sciences, Princeton University, Princeton, NJ 08544, USA*
[3]*Department of Physics and Astronomy, University of Pittsburgh, Pittsburgh, PA 15260, USA*
[4]*California Institute of Technology, Pasadena, CA 91125, USA*
[5]*Laboratoire d'Astrophysique de Marseille, France*
[6]*NOAO Gemini Science Center, 950 North Cherry Avenue, Tucson, AZ 85719, USA*

Accepted 2008 October 2. Received 2008 September 11; in original form 2008 April 2

ABSTRACT

We present a multi-epoch quantitative spectroscopic analysis of the Type IIn supernova (Type IIn SN) 1994W, an event interpreted by Chugai et al. as stemming from the interaction between the ejecta of a SN and a $0.4\,M_\odot$ circumstellar shell ejected 1.5 yr before core collapse. During the brightening phase, our models suggest that the source of optical radiation is not unique, perhaps associated with an inner optically thick cold dense shell and outer optically thin shocked material. During the fading phase, our models support a *single* source of radiation, an hydrogen-rich optically thick layer with a near-constant temperature of ∼7000 K that recedes from a radius of 4.3×10^{15} at a peak to 2.3×10^{15} cm 40 d later. We reproduce the hybrid narrow-core broad-wing line profile shapes of SN 1994W at all times, invoking an optically thick photosphere exclusively (i.e. without any external optically thick shell). In SN 1994W, slow expansion makes scattering with thermal electrons a key escape mechanism for photons trapped in optically thick line cores, and allows the resulting broad incoherent electron-scattering wings to be seen around narrow-line cores. In SNe with larger expansion velocities, the thermal broadening due to incoherent scattering is masked by the broad profile and the dominant frequency redshift occasioned by bulk motions. Given the absence of broad lines at all times and the very low ^{56}Ni yields, we speculate whether SN 1994W could have resulted from an interaction between two ejected shells without core collapse. The high conversion efficiency of kinetic to thermal energy may not require a SN-like energy budget for SN1994W.

Key words: radiative transfer – stars: atmospheres – supernovae: individual: 1994W.

1 INTRODUCTION

Understanding the diversity of supernova (SN) spectra and light curves is a considerable challenge. Although some SN classes suffer less and less ambiguity, as in the thermonuclear incineration of a Chandrasekhar-mass white dwarf leading to a Type Ia SN, or as in the collapse of the degenerate Chandrasekhar-mass Fe or O/Ne/Mg core of a massive star leading to Type II or Ib/c SNe, a unified picture of stellar explosions is compromised by the growing number of atypical SNe that emerge from deeper and more frequent searches for transient phenomena in the local and distant Universe. One such type of peculiar SNe is 'n'-suffixed (i.e. IIn, Ibn, Ian), in reference to their atypical narrow-line profiles. This suggests that despite the bright, SN-like, visual display, the expansion rate of the radiating layer is small, i.e. of a few $100\,km\,s^{-1}$, in contrast with the large ejecta velocities, of a few $1000\,km\,s^{-1}$, associated with SN explosions. Paradoxically, these events can boast a huge bolometric luminosity – a few $10^9\,L_\odot$ sustained for weeks (as in SN 1994W) but associated with a spectral energy distribution (SED) typical of a 10,000 K blackbody, hence implying 'photospheric' radii of a few 10^{15} cm [$L \sim 2 \times 10^9 (R_{15})^2 (T_4)^4\,L_\odot$, where R_{15} is the radius in units of 10^{15} cm and T_4 is the temperature in units of 10^4 K].

All SN ejecta yield photospheric radii of 10^{15} cm a few weeks after explosion, but the remarkable property of Type IIn SNe is that they achieve this with an apparent slow expansion. The common interpretation is that Type IIn SNe interact with material present in the direct environment of the exploding star, forming the 'photosphere' where that external material resides, at a few 10^{15} cm. If its mass is of the order of the ejecta mass, this outer material can cause a significant deceleration of the ejecta, with an efficient conversion of kinetic energy into internal and radiative energy.

The narrow-line cores are accompanied, in a subset of Type IIn SNe, by broad (and symmetric) line wings which are generally interpreted as arising from multiple electron scattering of line photons in the circumstellar (CS) shell with which the ejecta collide

★E-mail: luc@as.arizona.edu

© 2009 The Authors. Journal compilation © 2009 RAS

(Chugai 2001). These optical 'peculiarities' are also often associated with the detection of X-ray and/or radio emission, as well as significant spectral variations. Although interaction is evident in many SNe (see e.g. Chevalier & Fransson 1994; Fransson, Lundqvist & Chevalier 1996; Chevalier & Fransson 2003), Type IIn SNe are objects in which the interaction is central, and perhaps 'makes' the SN (i.e. the interaction can increase the luminosity so that it is easier to detect).

Given the rich mass-loss history and the many alternate channels of evolution, massive stars are the prime candidates for such interactions, in particular the hydrogen-rich, Type II, SNe. A few well-documented examples that reveal the wealth and the diversity of phenomena hosted by such IIn events are SN 1988Z (Stathakis & Sadler 1991; Turatto et al. 1993; van Dyk et al. 1993; Chugai & Danziger 1994; Fabian & Terlevich 1996; Aretxaga et al. 1999; Williams et al. 2002; Schlegel & Petre 2006), SN 1994W (Tsvetkov 1995; Sollerman, Cumming & Lundqvist 1998, hereafter SCL; Schlegel 1999; Chugai et al. 2004a, hereafter C04), SN 1995G (Pastorello et al. 2002; Chugai & Danziger 2003), SN 1995N (Fox et al. 2000; Fransson et al. 2002; Chandra et al. 2005; Zampieri et al. 2005; Mucciarelli et al. 2006), SN 1997eg (Salamanca, Terlevich & Tenorio-Tagle 2002; Hoffman et al. 2008) and SN 1998S (Bowen et al. 2000; Fassia et al. 2000; Gerardy et al. 2000; Leonard et al. 2000; Liu et al. 2000; Anupama et al. 2001; Chugai 2001; Fassia et al. 2001; Lentz et al. 2001; Chugai et al. 2002; Pooley et al. 2002; Pozzo et al. 2004; Fransson et al. 2005; Pozzo et al. 2005). Despite the common Type IIn SN, the above sample of SNe do not boast a uniform set of properties, some being bright for weeks, some for months or even years; some showing a clear brightness plateau after peak, others fading by a few magnitudes in just a few weeks, etc. Objects classified as 'n'-type SNe are in fact shaking the common understanding of what makes a SN.

The Type IIn SN 2006gy, the most luminous SN ever seen, may have originated from a pair-instability explosion (Ofek et al. 2007; Smith et al. 2007; Smith & McCray 2007), or consecutive pair-instability pulsations (Woosley, Blinnikov & Heger 2007) in a supermassive star. Recently, SN 2006jc also joined SN 1999cq and SN 2002ao to consolidate the rare SN Ibn type, characterized by narrow lines of helium instead of hydrogen, an interpretation that conflicts with the notion that pre-SN mass ejections are generally associated with hydrogen-rich stars [e.g. luminous blue variables (LBVs), see Davidson & Humphreys 1997; Matheson et al. 2000; Foley et al. 2007; Pastorello et al. 2007]. Interaction with CS material has also been invoked in the Type Ia SN 2002ic following the observations of narrow hydrogen-line emission in the optical spectrum (Hamuy et al. 2003; Chugai & Yungelson 2004; Chugai, Chevalier & Lundqvist 2004b; Deng et al. 2004; Kotak et al. 2004; Wang et al. 2004; Wood-Vasey, Wang & Aldering 2004; Benetti et al. 2006; Han & Podsiadlowski 2006; Wood-Vasey & Sokoloski 2006; Chugai & Chevalier 2007).

Modelling such an interaction is a complicated radiation hydrodynamics problem, in which the uncertainties in the properties of both shells prior to the interaction add to those of the interaction itself. The diversity of observations suggests that a similar diversity is to be found in the circumstances of the interaction. Focusing from now on the massive star progeny, the outer, CS, material may arise from the pre-SN steady-state wind mass loss, an LBV outburst, perhaps a violent pair-instability pulsation, or some yet unidentified ejection mechanism occurring recurrently (and without core collapse) or immediately prior to core collapse. The inner shell that rams into this CS shell may arise from a core-collapse SN explosion (which may be neutrino, acoustic or magnetically driven; see Woosley & Janka 2005 for a review), a pair-instability pulsation, a pair-instability explosion or some other form of explosion. For a SN-like display to occur, the inner shell must be fast to catch up with the CS material and cause a violent shock. A short delay between the two mass ejections will raise the probability for detection. A large kinetic energy is involved, and the conversion of kinetic to thermal energy supplies the internal/radiant energy inferred from the bolometric light curve. Moreover, mass/energy distribution of both shells may not be spherical (Leonard et al. 2000; Hoffman et al. 2008) and thus, viewing effects may complicate further the dynamics of the interaction and the interpretation of the emitted light. Finally, the bolometric display may be altered by an additional contribution from radioactive decay of unstable isotopes, which are normally associated with SN ejecta.

An attempt to quantitatively interpret the Type IIn SN 1994W was undertaken by C04 who performed radiation-hydrodynamics and radiative-transfer calculations to model very high quality multi-epoch spectroscopic and photometric observations (see also SCL). For SN 1994W, C04 associate the narrow-line core with an expanding CS envelope. The broad-line wings arise from a combination of shocked cool gas in the forward post-shock region, and multiple electron scattering in the CS envelope. They associate the absence of broad P Cygni line profiles with obscuration by an optically thick cold dense shell (CDS) that forms at the interface of SN ejecta and a CS envelope. They infer a CS envelope with a particle density $n \sim 10^9$ cm^{-3}, a radial extent of a few 10^{15} cm, an electron-scattering optical depth of $\gtrsim$2.5, explosively ejected $\sim$1.5 yr prior to the SN explosion. The light curve shows a rise time to peak of about 30 d (after the reference date 1994 July 14), followed by a slow decline by about two magnitudes until 110 d, and a sudden decline beyond that date (see Fig. 1 in SCL).

Despite all the complexities that surround this ejecta/CS envelope interaction, the inferred presence by C04 of an optically thick CDS suggests that the approach we follow for the modelling of photospheric-phase Type II-Plateau (II-P) SNe (Dessart & Hillier 2005a,b, 2006, 2008; Dessart et al. 2008) may also apply here. In this work, we provide insights into the spectroscopic and light-curve evolutions of SN 1994W between day 20 and 100, thus covering from $\sim$10 d before peak, through to the slow decline that follows, and ending 10 d before the steep bolometric fading.

The main results from this work are that although the outward-moving CDS is likely opaque until the peak of the light curve, the photosphere recedes in both mass and radius for post-peak times as the material cools and recombines. In this context, the sharp drop at 110 d is the transition to the nebular phase, when the ejecta/circumstellar material (CSM) is entirely optically thin, analogous to the end of the plateau phase in Type II-P SNe. We also find that the broad wings on the Balmer lines can be explained by the multiple electron scattering in the photosphere – we do not need multiple density structures to explain the observed spectrum.

In the next section, we discuss the reddening and distance used in our study of SN 1994W. In Section 3, we evaluate various timescales that characterize Type IIn SNe. We then summarize our modelling approach in Section 4, presenting the various approximations we make to mimic as best we can the complicated configuration of the interacting SN 1994W. In Section 5, we present the ejecta properties we infer from the modelling of the photometric and spectroscopic observations at multiple epochs during its optically bright phase. We reproduce the narrow-line core and the broad-line wings by invoking a single region of emission/absorption (the photosphere), rather than the CDS and CS-envelope configuration. In Section 6, we discuss the line formation process in our models

of SN 1994W, and emphasize the important role of electron scattering in some Type IIn SN photospheres that are characterized by low, and perhaps nearly constant, expansion velocities. We finally present our conclusions and discuss the implication of our results for interacting SNe in a more general context in Section 7.

2 REDDENING AND DISTANCE

Following SCL, we adopt a distance to SN 1994W of 25.4 Mpc which is based on $H_0 = 65\,\mathrm{km\,s^{-1}\,Mpc^{-1}}$ and the Virgo infall model of Kraan-Korteweg (1986). This is somewhat larger than the distance estimate of 18.0 Mpc by Gao & Solomon (2004) which used $H_0 = 75\,\mathrm{km\,s^{-1}\,Mpc^{-1}}$ and was corrected for motion of the Local Group. While the choice of distance will affect the adopted luminosity and inferred photospheric radii, other conclusions in this paper (including $T_{\rm phot}$) are not affected. The reddening is more problematical since it can affect the relative flux distribution. SCL find $E(B-V) = 0.17 \pm 0.06$ mag based on the equivalent width (EW) of the NaID doublet and its correlation with $E(B-V)$ while C04 estimate 0.15 mag from blackbody fits to spectra at several different dates. As the galactic extinction in the direction of SN 1994W is low, most of the reddening must be internal to the host galaxy (SCL). Our present model, particularly of spectra past the peak, supports the SCL reddening although values of 0.15 to 0.20 mag are also compatible with the observations. In this work, we employ a reddening of 0.15–0.17, but also explore the effects of reducing the reddening to 0.07 on day 21.

3 TIME-SCALES

A typical expansion velocity for SN 1994W, as measured from the narrow-line profiles, is $800\,\mathrm{km\,s^{-1}}$. We can use this to define an expansion time-scale using a typical photospheric radius of 4×10^{15} cm. This gives an expansion time-scale of 1.6 yr. As noted earlier, this, together with the large luminosity, and the difficulty of creating SNe with a low expansion velocity are reasons for the argument that the $800\,\mathrm{km\,s^{-1}}$ is not an intrinsic SN expansion velocity. C04 suggest it is the velocity of CS material that was ejected prior to the SN explosion. Alternatively, it could reflect the velocity of a shell of gas that has arisen from the interaction of CS gas with the SN ejecta. The largest red supergiants have radii of 10^{14} cm (see e.g. Levesque et al. 2005), significantly smaller than the inferred photospheric radius.

The light travel time across the SN is $2R/c \sim 3.1$ d. This is marginally significant, and indicates that the observed light curve will be averaged over this time-scale. The diffusion time is of the order of $\tau R/cn$, where n is the exponent of the power-law density. This will also have a significant impact on the observed light curve, although it is less clear whether it will affect our spectroscopic modelling in which we fix the luminosity at the base of the photosphere.

4 MODEL PRESENTATION

In hydrogen-rich environments, having an optically thick layer simplifies considerably the radiative transfer problem. The associated large bound-free opacities ensure that the radiation is thermalized before escaping through the photosphere – all photons at depth will be absorbed and re-emitted according to a blackbody distribution characterized by the local electron temperature, irrespective of the details of the interaction. Hence, we have a setup that is analogous to that of a typical stellar atmosphere. Not accounted for in this configuration is the potential contribution from the optically thin layers above the photosphere that have been shocked. These regions can contribute to the electromagnetic display directly, as they often do in the X-ray and radio ranges, or alter the photospheric conditions through the external irradiation. How well we reproduce the observations may be a gauge on how much these regions contribute to the total SN luminosity and affect the photospheric conditions. In the case of SN 1994W, we can reproduce the observations after the peak by photospheric radiation alone. However, before the peak we cannot fully reproduce the observations accurately, possibly indicating that optically thin gas makes an important contribution. Alternatively, neglected effects such as departures from spherical symmetry and time-dependent effects may be important at such early times (Dessart & Hillier 2008).

We model the observations with the non-local thermodynamic equilibrium (non-LTE) steady-state one-dimensional radiative transfer code CMFGEN (Hillier & Miller 1998; Dessart & Hillier 2005a) which solves self-consistently the radiative transfer equation and the statistical equilibrium equations under the constraint of radiative equilibrium. Of particular relevance for this work, CMFGEN treats accurately the electron-scattering source function. With our adopted distance and a reddening of $E(B-V) = 0.17$ mag, a blackbody emitter, with a temperature of 10^4 K and a radius of 10^{15} cm, would have an observed V-band magnitude of $\sim$14.5, in close agreement with the observed value around day 50 (see Fig. 1 of SCL98). We therefore started our model analysis with a typical Type II-P SN model just prior to hydrogen recombination (as in Dessart & Hillier 2005a, 2006; Dessart et al. 2008), and modified the radius and luminosity to agree with the above brightness estimate. We also adopt a supergiant-like composition, i.e. $X_{\rm H} = 0.55$, $X_{\rm He} = 0.44$, $X_{\rm C} = 5.3 \times 10^{-4}$, $X_{\rm N} = 2 \times 10^{-3}$, $X_{\rm O} = 2.8 \times 10^{-3}$. Metal abundances are taken at the solar value. We use the same model atom for all investigations presented here, with H I, He I, C I, C II, N I, N II, Na I, Mg II, Si II, Ca II, Al II, Al III, O I, O II, S II, S III, Cr II, Cr III, Mn II, Mn III, Ti II, Ti III, Co II, Co III, Ni II, Ni III, Fe II, Fe III and Fe IV (details on the levels treated are omitted, but our choice is such that increasing the number of levels does not alter the computed ejecta properties nor the emergent synthetic spectrum).

The atomic data come from a wide variety of sources, the Opacity Project (Seaton 1987; The Opacity Project Team 1995, 1997), the Iron Project (Hummer et al. 1993; Kurucz & Bell 1995; Pradhan et al. 1996) and the Atomic Spectra Data base at the National Institutes of Standards and Technology (NIST) Physical Laboratory being the principal sources. Most of the Kurucz data were obtained directly from the Center for Astrophysics (Kurucz 1988, 2002). Individual sources of atomic data include the following: Bautista & Pradhan (1997), Becker & Butler (1995), Butler, Mendoza & Zeippen (1993), Fuhr, Martin & Wiese (1988), Kingdon & Ferland (1996), Luo & Pradhan (1989), Luo et al. (1989), Mendoza (1983), Mendoza et al. (1995), Nahar (1995, 1996), Nahar & Pradhan (1996), Neufeld & Dalgarno (1987), Nussbaumer & Storey (1983, 1984), Peach, Saraph & Seaton (1988), Storey (private comm., 1988), Tully, Seaton & Berrington (1990), Wiese, Smith & Glennon (1966); Wiese, Smith & Miles (1969) and Zhang & Pradhan (1995, 1997).

Dynamical simulations by Chevalier (1982) and C04 suggest that in this context a very steep density fall-off would prevail above the CDS, while the velocity would be decreasing from the CDS outward into the shocked CS envelope. Adopting a power-law density distribution of the form $\rho(R) = \rho_0 (R_0/R)^n$, where ρ_0 and R_0 are, respectively, the density and the radius at the optically thick model

Table 1. Model characteristics for SN 1994W. For each date in our sample of observations, we provide the following CMFGEN model parameters: base comoving-frame luminosity L_{CMF,R_0} and emergent observer-frame luminosity $L_{\mathrm{OBS},R_{\mathrm{Max}}}$ (in $10^8\,\mathrm{L}_\odot$), photospheric conditions describing the electron temperature T_{phot} (in K), the radius R_{phot} (in 10^{15} cm), the velocity V_{phot} (in $\mathrm{km\,s^{-1}}$), the mass density (in $10^{-14}\,\mathrm{g\,cm^{-3}}$) and the free-electron density $N_{\mathrm{e,phot}}$ (in $10^9\,\mathrm{cm^{-3}}$). In all models, a density exponent $n = 10$ characterizes the density law $\rho(R) = \rho_{\mathrm{phot}}(R_{\mathrm{phot}}/R)^n$. M_V and m_V correspond to V-band absolute, and reddened plus distance-diluted (using a distance of 25.4 Mpc and a reddening of 0.17 with $R_V = 3.1$), synthetic magnitudes. Because there are clear inconsistencies between our model and the observations on days 21 and 31, we quote the corresponding model parameters on those dates only for completeness – we do not suggest that they accurately describe SN 1994W on these two dates.

Day YY–MM–DD	Phase[a] Days	L_{CMF,R_0} ($10^8\,\mathrm{L}_\odot$)	$L_{\mathrm{OBS},R_{\mathrm{Max}}}$ ($10^8\,\mathrm{L}_\odot$)	T_{phot} (K)	R_{phot} (10^{15} cm)	V_{phot} ($\mathrm{km\,s^{-1}}$)	ρ_{phot} ($10^{-14}\,\mathrm{g\,cm^{-3}}$)	$N_{\mathrm{e,phot}}$ ($10^9\,\mathrm{cm^{-3}}$)	M_V synthetic	M_V synthetic
1994-08-04[b]	21.5	66.0	61.7	10350	2.86	830	0.82	3.3	−18.78	13.37
1994-08-14[b]	31.5	66.0	61.7	10350	2.86	830	0.82	3.3	−18.78	13.37
1994-09-01[c]	49.5	47.0	42.0	7480	4.32	830	0.62	2.1	−18.80	13.75
1994-09-09	56.9	27.0	24.0	7450	3.33	840	0.84	2.7	−18.37	14.18
1994-10-01	79.5	9.8	8.7	6310	2.37	790	2.7	5.2	−17.61	14.94
1994-10-11	89.5	9.0	8.0	6020	2.32	712	7.6	7.5	−17.59	14.96

[a]Days after 14.0 July 1994.
[b]So-called hot model, used to fit observations on the 4th and the 14th of August, both poorly.
[c]So-called cool model, used to fit observations on the 4th and on the 14th of August (but poorly for both dates), and on September 1 (satisfactorily).

base, we enforce a steep density fall off by taking a density exponent n equal to 10. Flatter density distributions, as in a wind solution with $n = 2$, yield optical line fluxes that are systematically stronger than observed. Steeper density distributions lead to weaker line fluxes and/or absorption lines. With our current approach and from extensive experimentation, we indeed find that the density distribution at the photosphere has to be steep, in fact comparable to that used for the modelling of Type II-P SNe.[1]

The transfer equation solver in CMFGEN requires *monotonically* expanding ejecta. In SN ejecta, the steep density profile tends to make the line and continuum formation quite confined in space, so the material properties on a large scale tend to matter little compared to the properties in the immediate vicinity of the photosphere. In our approach, we assume homologous expansion for simplicity, and adjust the ejecta velocity to match the observed line profile widths. Note that in the line transfer problem, it is the magnitude of the velocity gradient at the photosphere, rather than its sign, that matters (see Sobolev 1960; Castor et al. 1975). Obviously, this is a numerical convenience and we do not suggest that in reality the velocity increases linearly with radius outwards, although it might. Later on, to test the dependence on the velocity gradient at the photosphere, we try out different values for the exponent β entering our parametrized velocity law, i.e. $V(R) = V_0(R/R_0)^\beta$, with β varying from 1 (homologous expansion) to 0.2, and 0.01 (near-constant velocity ejecta; here, V_0 is the model-base velocity). Moreover, to ensure the radiation is thermalized at the inner boundary, we extend our grid inwards to a radius where the Rosseland optical depth is ∼100. Finally, when comparing to observations, we first redden our synthetic spectra with the Cardelli law (Cardelli et al. 1989), and then adjust the synthetic flux (at most by a few per cent) to get the desired overlap. This is a convenience, equivalent to a change in photospheric radius or distance (scaling with the square root of that scaling factor), that saves us from re-running a model that would otherwise have the same properties and spectrum (see discussion in Dessart & Hillier 2005a).

5 RESULTS

We have performed a spectroscopic analysis of the data presented in SCL and C04 for the observations taken on 1994 August 4 and 14 (Section 5.1), September 1 and 9 and October 1 and 11 (the last four dates are presented in Section 5.2), which correspond to days 21, 31, 49, 57, 79 and 89 after 1994 July 14 (we adopt that reference date for compatibility with SCL, who associate it with the 'optical outburst' of SN 1994W).

These observations correspond to a phase of optical brightening prior to day 30, followed by an 80-day long phase of slow optical fading ($\Delta m \sim 1.5$ mag), eventually followed by a sudden fading of the SN past day 110. We omit from our sample the lower quality data obtained on day 18, as well as the late time, nebular spectrum obtained on day 121. Model parameters for each epoch are stored in Table 1, although we stress that the results for days 21 and 31 are uncertain, and given for completeness only.

All observed spectra have been de-redshifted assuming a heliocentric velocity of $1249\,\mathrm{km\,s^{-1}}$ (C04). Using the Cardelli et al. (1989) law, we redden our synthetic spectra to match observations, using $E(B - V) = 0.17$ mag, unless otherwise stated. We also provide, as online material, the list of all lines between 3200 and 10 500 Å that contribute an EW (approximate since computed using the Sobolev approximation, and quoted merely to indicate the main contributors; Sobolev 1960) of at least 1 Å (in absolute value). Each line, in absorption, emission or both, may appear as a single feature, or may overlap with neighbouring lines to yield a complicated feature.

5.1 Observations pre-peak optical brightness: days 21 and 31

To highlight the spectroscopic peculiarities of SN 1994W, we first review the spectral evolution of Type II-P SNe which are governed by ejecta cooling and the increased effects of metal-line blanketing. The SED is blue during the first 10 d after shock breakout and reddens dramatically as hydrogen recombines in the ejecta. Balmer lines are the strongest lines at all times, initially accompanied by He I lines (5875 Å is the most conspicuous, but other optical He I lines are present) and then by Fe II lines. These proceed in a monotonic sequence, so that He I and Fe II lines are not seen simultaneously.

In Type IIn SNe, and by contrast with Type II-P SNe, such smooth and monotonic evolution does not systematically hold. The spectrum of SN 1994W on day 21 shows the simultaneous presence of both Fe II and He I optical lines (with absorption and emission components), in combination with a blue continuum. To illustrate this peculiarity, we show in Fig. 1 three different fits to the

[1] Note that recombination to a neutral state may attenuate the spectral dependence on the density distribution above the photosphere.

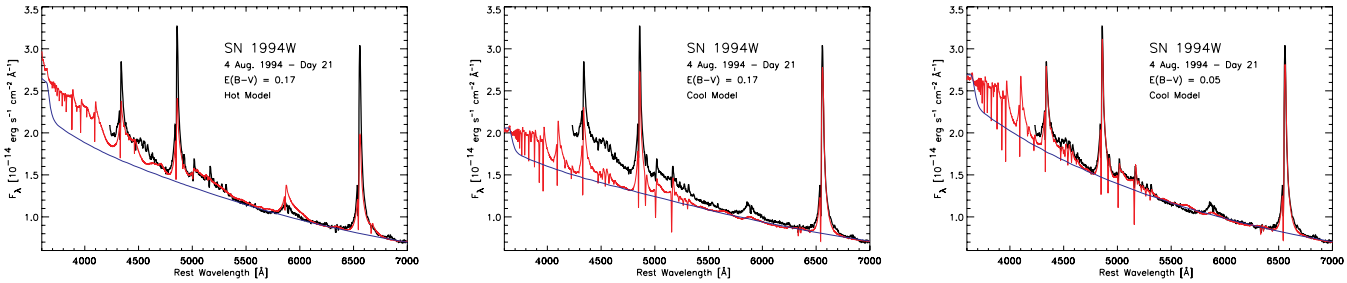

Figure 1. Left-hand panel: comparison between the reddened [$E(B-V) = 0.17$ mag] full (red) and continuum-only (blue) synthetic spectrum and the observations of SN 1994W on the 1994 August 04 (day 21; black). The synthetic flux is scaled by a factor of 1.06 to adjust to the absolute level of the observed flux. The ejecta ionization predicted with our model parameters reproduces the slope of the SED adequately, but it overestimates the strength of He I 5875 Å and underestimates the strength of Fe II lines. Note, however, the good fit to the Balmer lines. Middle panel: same as left-hand panel, but now with a cooler model used to fit observations on 1994 September 01 (see Fig. 3; we use a flux scaling of 0.93). Note the bad fit to the SED slope, but the improved fit to observed line profiles. Right-hand panel: same as middle panel, but using a reddening of 0.05 instead of 0.17. Now, the fit to both the continuum and lines is good. What causes this combination of blue continuum and lines of low-ionization species is unclear. Being short-lived, it may be related to the shocked material above the photosphere, rather than to large changes in photospheric conditions. Reducing the reddening is only a proxy for getting a good fit, for exploratory purposes, to the data taken on this date.

observations of SN 1994W on day 21. In the left-hand panel, we use a 'hot model' with the following properties: $R_{\rm phot} = 2.86 \times 10^{15}$ cm, $V_{\rm phot} = 830\,{\rm km\,s^{-1}}$, $T_{\rm phot} = 10\,350$ K, $\rho_{\rm phot} = 8.2 \times 10^{-15}\,{\rm g\,cm^{-3}}$, $N_{\rm e,phot} = 3.3 \times 10^{9}\,{\rm cm^{-3}}$ and $L_{{\rm OBS},R_{\rm Max}} = 6.17 \times 10^{9}\,{\rm L_{\odot}}$. (We have scaled the synthetic flux by a factor of 1.06.) The model ejecta are relatively hot, nearly fully ionized (only helium is partially ionized just above the photosphere). The observed shape of the SED is approximately matched, but there are severe discrepancies. He I 5875 Å is too strong, in both the emission strength and width (note that using a solar composition for hydrogen and helium reduces, but does not resolve, this discrepancy). Numerous lines around 4500 Å (Ti II and Fe II), as well as around 5200 Å (mostly Fe II), are strongly underestimated. Balmer lines are underestimated in strength, but well fitted in width. The absorption at $\sim -800\,{\rm km\,s^{-1}}$ from line centre is also well reproduced.

In the middle panel of Fig. 1, we show the fits to the same observations, but using a cooler model ($T_{\rm phot} = 7480$ K; we have scaled the synthetic flux by a factor of 0.93), the one that fits the observations of SN 1994W on 1994 September 1 (see Table 1 for characteristics). The slope of the synthetic SED is now in greater disagreement, but the ionization seems more adequate, as we predict all the observed lines, merely shifted vertically due to a redder/weaker continuum. As an experimentation, we reduced the reddening from 0.17 to 0.05 and, as evident in the right-hand panel of Fig. 1, the fits to both the continuum and the lines become excellent. We do not support this reddening, as it is incompatible with past works (SCL, C04) and the modelling done for later dates, even within the uncertainties. But, this experimentation suggests that two distinct regions contribute, one to form a blue nearly featureless SED (as we do not see high-ionization lines) and another to produce the lines from low-ionization species (Fe II). This is a distinctive feature of SN 1994W, not seen in Type II-P SNe, and only visible on this day and day 31.

On day 31, the optical spectroscopic observations of SN 1994W undergo a drastic and atypical change, with the SED becoming bluer (C04 stress that this change is genuine, and not the result of a poor relative flux calibration), the narrow lines of Fe II appearing weaker at, e.g., 5018 and 5169 Å. We identify H I Balmer lines, He I 5875 Å, He I 6678 Å, and He I 7065 Å and Mg II 7877–7896 Å. In the cool model (same as that used to model observations on the 1994 September 1) shown in the bottom panel of Fig. 2, the Mg II

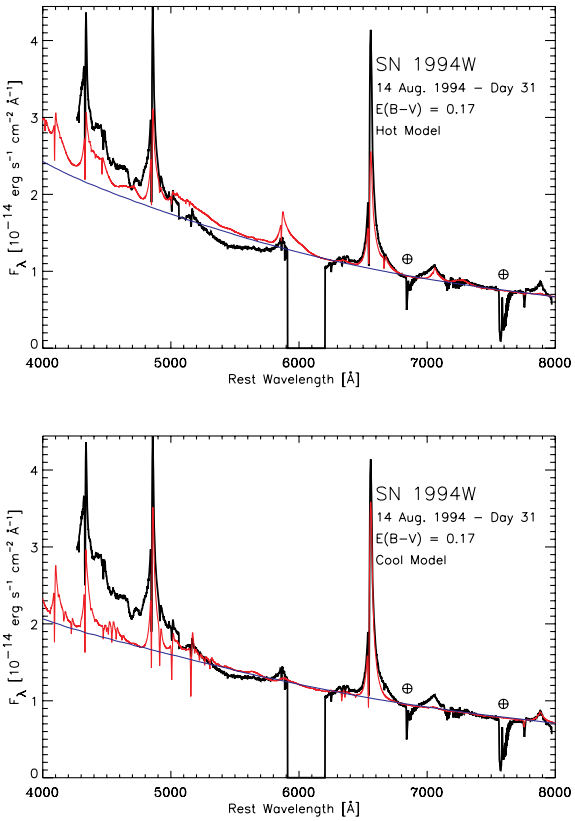

Figure 2. Top panel: comparison between the reddened [$E(B-V) = 0.17$ mag] full (red) and continuum-only (blue) synthetic spectra for a hot model and the observations of SN 1994W on 1994 August 14 (day 31; black). The synthetic flux is scaled by a factor of 1.37 to adjust to the absolute level of the observed flux. Bottom panel: same as top panel, but now with the (cooler) model employed for the observations of September 1 (we apply a flux scaling of 1.2). Note how the Mg II 7877–7896 Å (He I 7065 Å) line is well fitted with the cool (hot) model, but not both at the same time, suggesting two different sites/mechanisms for the origin of these lines. By contrast, the electron-scattering wings are well reproduced in both models, despite the ejecta ionization changes.

lines and He I 5875 Å are well reproduced, but He I 7065 Å is not. By contrast, in the hot model (same as the hot model used on day 21 presented above) shown in the top panel, the reverse is true.

Overall, our fits to these pre-peak brightness observations are very poor. The apparent increase in ionization between days 21 and 31 is a unique feature of SN 1994W, never quite seen in standard SN ejecta (of any type), which are governed by the cooling associated with expansion, typically mitigated by the release of stored internal energy. The non-monotonic SED evolution of SN 1994W between days 21 and 31, and the simultaneous presence of lines suggestive of both high and low ejecta temperatures point towards two distinct radiating regions (or material), of distinct properties.

As there are clear inconsistencies between our model and the observations on days 21 and 31, the quoted model parameters do not accurately describe SN 1994W on these two dates. It is possible, for example, that the photospheric radius and temperature derived for day 49 also apply at the earlier dates; the extra luminosity would then arise from an optically thin, and more highly ionized, outer region.

5.2 Observations post-peak optical brightness: days 49, 57, 79 and 89

From day 49 onwards, the visual brightness of SN 1994W decreases slowly, from ∼13.5 on that day down to ∼15 on day 110 (SCL). Over that time, the observed spectral evolution is smooth and slow, analogous to that of Type II-P SNe during the plateau phase, and our fits are satisfactory. We present synthetic fits to observations in Fig. 3 for day 49, in Fig. 4 for day 57, in Fig. 5 for day 79 and in Fig. 6 for day 89. We also give the corresponding model parameters in Table 1. These spectra are dominated by lines of low-ionization species, such as H I, Fe II, Na I, Ca II, Mg II, with He I 5875 Å disappearing after day 59 (see tables provided as online material for

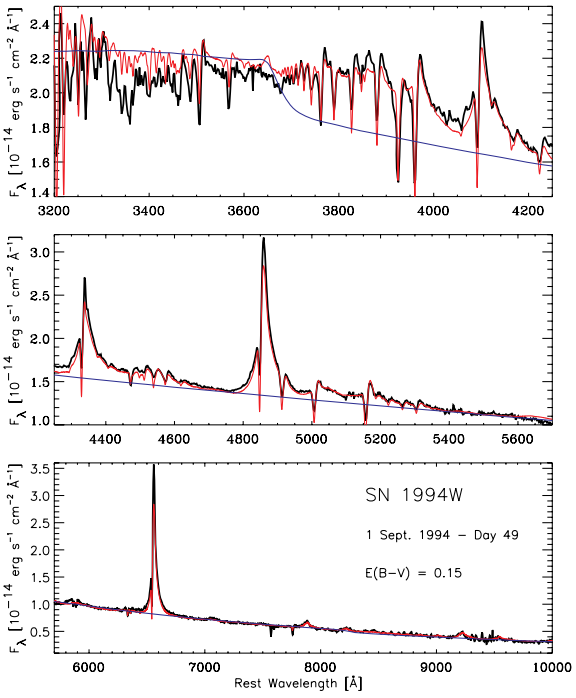

Figure 3. Comparison between the reddened [$E(B-V) = 0.15$ mag] full (red) and continuum-only (blue) synthetic spectra and the observations of SN 1994W on 1994 September 01 (day 49; black). The synthetic flux is scaled by a factor of 0.87 to adjust to the absolute level of the observed flux.

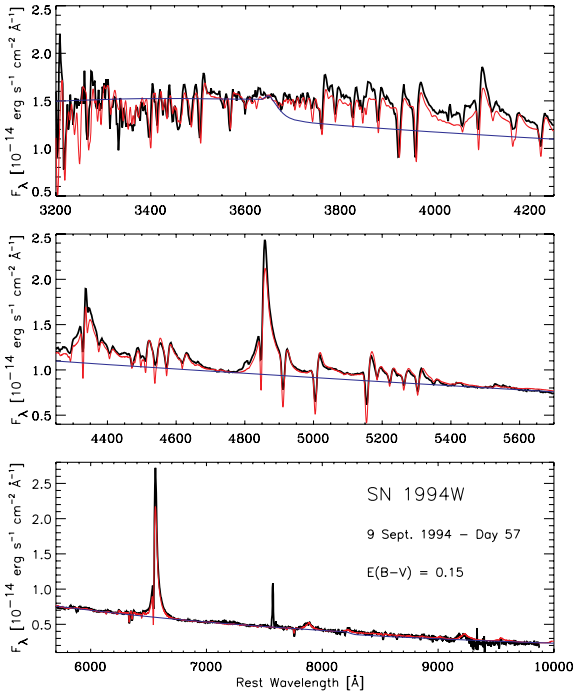

Figure 4. Comparison between the reddened [$E(B-V) = 0.15$ mag; this is to reduce a slight discrepancy around 4000–5000 Å] full (red) and continuum-only (blue) synthetic spectra and the observations of SN 1994W on 1994 September 09 (day 57; black). The synthetic flux is scaled by a factor of 1.02 to adjust to the absolute level of the observed flux.

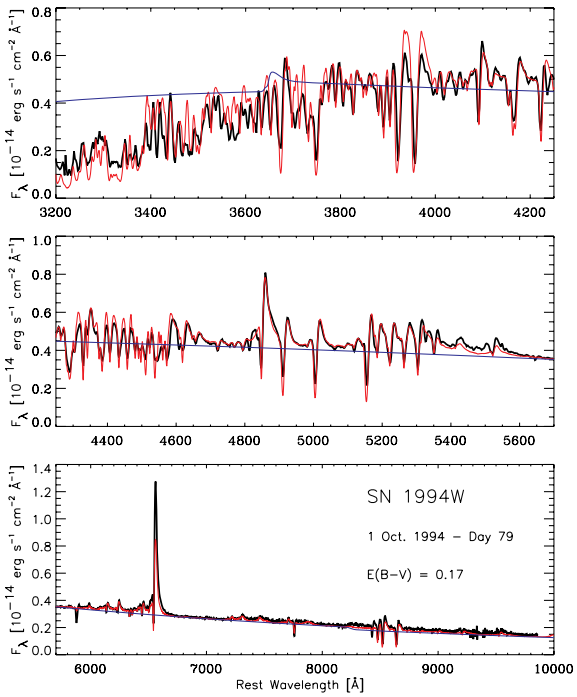

Figure 5. Comparison between the reddened [$E(B-V) = 0.17$ mag] full (red) and continuum-only (blue) synthetic spectra and the observations of SN 1994W on 1994 October 01 (day 79; black).

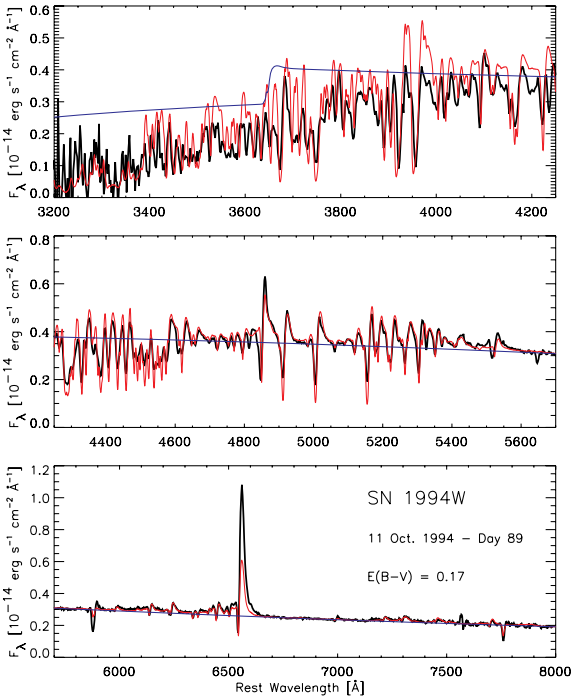

Figure 6. Comparison between the reddened [$E(B-V) = 0.17$ mag] full (red) and continuum-only (blue) synthetic spectra and the observations of SN 1994W on 1994 October 11 (day 89; black). The synthetic flux is scaled by a factor of 0.87 to adjust to the absolute level of the observed flux.

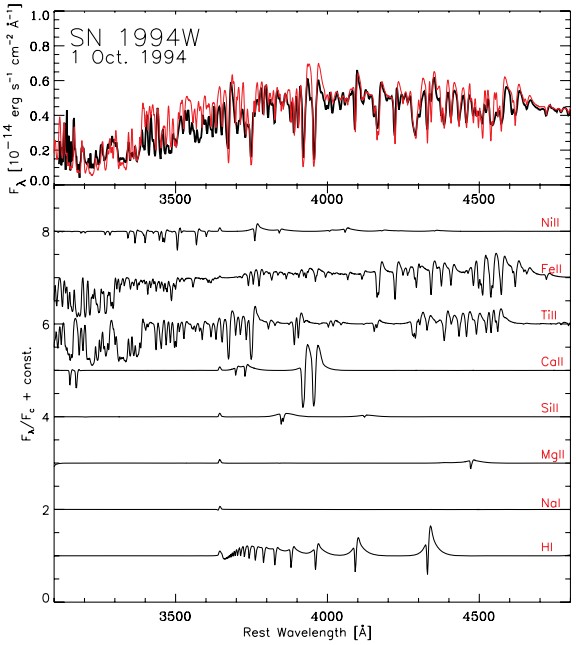

Figure 7. Top panel: comparison between the reddened [$E(B-V) = 0.17$ mag] synthetic spectrum (red) and the observations of SN 1994W on 1994 October 01 (day 79; black), between 3100 and 4800 Å. Bottom panel: rectified synthetic spectra for the model shown at top, but including bound–bound transitions only of the individual species labelled on the right-hand side.

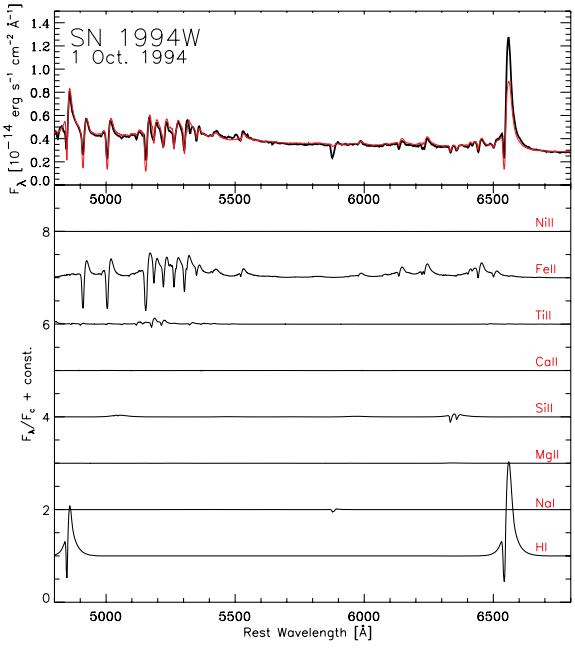

Figure 8. Same as Fig. 7, but for the range 4800 to 6800 Å.

a complete census of all contributing lines). Observations and our synthetic SED now agree well, suggesting both lines and continuum form in the same region of space, i.e. under similar conditions of density and temperature. As on days 21 and 31, Balmer lines continue to show conspicuous narrow-line cores with extended wings. Our fits to the line cores tend to be underestimated (by up to a factor of 2 on day 89), but we can reproduce well the strength and width of the profile wings. These profile wings stem from multiple electron-scattering events of photons originally trapped in the line core, a phenomenon, in our approach, which occurs in the photospheric region (see Section 6). We also predict the absorption dip at $\sim -700\,\mathrm{km\,s^{-1}}$, coincident for all lines within $\pm 100\,\mathrm{km\,s^{-1}}$. This latter feature is also associated here with absorption internal to the photospheric region. We go back to these two intriguing characteristics in Section 6. The underestimate of the narrow-line Hα flux could be due to the neglect of time-dependent effects (Dessart & Hillier 2008), or might be due to a change in the density distribution within the SN envelope (as characterized by the exponent n).

In the top panel of Figs 7–9, we reproduce the fit shown in Fig. 5 but this time zooming in on the 3100–4800 Å region (Fig. 7), the 4800–6800 Å region (Fig. 8) and the 6800–9800 Å region (Fig. 9). Moreover, in the bottom panels, we present the contributions of individual species by plotting the rectified synthetic spectra obtained by accounting for bound–bound transitions of individual species, labelled at the right-hand side. At such a late time, besides Balmer and a few isolated Mg II, Na I, Si II and Ca II lines, we note the presence of a forest of Fe II and Ti II lines blueward of ∼4500 Å. The strengthening contribution of line emission and absorption is also evident in Figs 3–6, where the blue curve describing the continuum SED departs more and more with time from the red curve including all absorption and emission processes, the more so at shorter wavelengths. This makes the continuum level difficult to assess, and the comparison with a blackbody increasingly inadequate. This complication should be kept in mind when using blackbody arguments.

Over this period from day 49 to 89, which covers the visual fading of the SN by ∼1.3 mag, we find a modest reduction in the photospheric temperature, of ∼1400 K ($\lesssim$20 per cent), but a large reduction in the photospheric radius, by $\sim 2 \times 10^{15}$ cm (a factor of 2

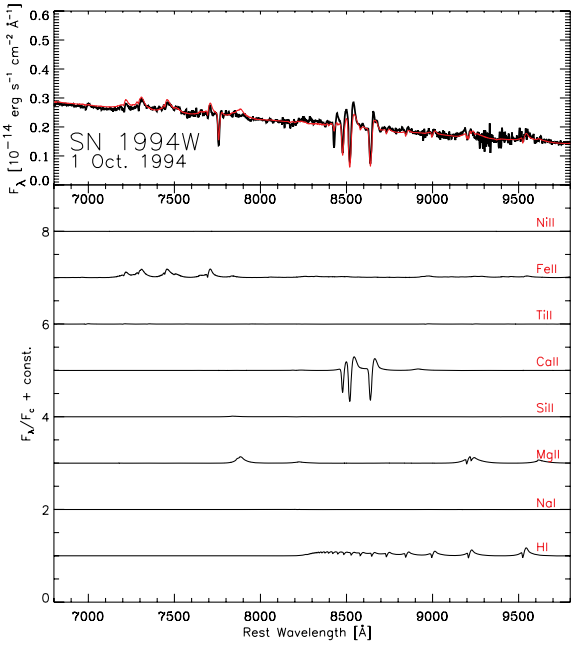

Figure 9. Same as Fig. 7, but for the range 6800 to 9800 Å.

reduction compared to the value on day 49). In the observer's frame and over these 40 d, this corresponds to a motion of the photosphere inward at an average velocity of $\sim$6000 km s^{-1}. This is analogous to the reduction in the photospheric radius at the end of the plateau phase of Type II-P SNe, in which an ejecta extending out to a few times 10^{15} cm become entirely optically thin in just $\sim$2 weeks. Heuristically, the photometric fading and the strongly correlated *B* and *V* magnitudes support a reduction in the photospheric radius and a fairly constant photospheric temperature, respectively.

The dynamics of the CDS is that of linear expansion with time (C04). Our findings suggest that the photosphere does not track the CDS, otherwise this linear expansion in time at near constant photospheric temperature would correspond to a phase of brightening. We instead observe a fading of the SN over that period. C04 associate the broad wings with the CDS deducing an expansion velocity of 4000 km s^{-1}. Over 100 d, the CDS would expand by $\sim 3.5 \times 10^{15}$ cm, compared to our inferred reduction in $R_{\rm phot}$ of $\sim 2 \times 10^{15}$ cm.

Our models suggest that as time progresses, the photosphere recedes to deeper and deeper layers in a cold shell – probably the SN ejecta (or more generally the inner shell) but possibly also associated with the CDS initially. We surmise that, as time goes on, the emitting material radiates and expands sufficiently to cause ejecta cooling and recombination. The photosphere is completely slaved to the layer of ionized material above which free electrons are too scarce to provide any sizable optical depth. Lines, which form above the photosphere, also tend to track this region of high density and high ionization, in particular those that form primarily through recombination, e.g. Balmer lines. Since the ejecta are hydrogen-rich, this occurs at a temperature of $\sim$7000 K, and that temperature is essentially fixed. With further cooling, it is not the temperature of the photosphere but instead the radius of the photosphere that adjusts, shrinking to deeper layers.

This process has already been identified as the primary cause for the plateau phase of Type II-P SNe: the photospheric temperature remains fixed at $\sim$7000 K, with a recession in mass coordinate of the photosphere, compensated in this case by the fast expansion of the ejecta so that the photospheric radius remains roughly constant during that phase (see fig. 16 in Dessart et al. 2008). The end of the plateau phase and the fast drop into the nebular phase will correspond to the time when the inward-travelling photosphere no longer sustains a high enough density and ionization to remain optically thick. In other words, the end of the plateau phase would not correspond to the time when the CDS reaches the outer edge of the outer shell (C04), but to the time when the photosphere eventually reaches the cold, fully recombined, inner layers of the SN ejecta/inner shell.

Since the CDS seems to be optically thin after the epoch of peak brightness, it cannot obscure the SN ejecta buried at depth. The absence of broad SN-like spectral features may then result from the ejecta deceleration by the reverse shock. Some deceleration is expected if conversion of kinetic energy into internal energy is to power the SN brightness, but the exact circumstances that cause the absence of ejecta material with velocity at the photosphere greater than $\sim$800 km s^{-1} at all times are unclear. Even at day 121, in the nebular phase, the expansion velocities indicated by Hα are consistent with an expansion of $\sim$800 km s^{-1} (C04). This is consistent with the idea that we are observing a shell of material moving with near constant velocity, but which is now in the nebular phase.

6 DISCUSSION OF LINE PROFILE FORMATION AND THE ELECTRON-SCATTERING WINGS

6.1 Observational aspects

The distinctive feature of Type IIn SNe is the presence of narrow, and usually symmetric, line cores at all times. In some cases, as for SN 1994W, these are accompanied by broad, and relatively symmetric line wings, giving the overall line profile a triangular shape (see Fig. 10). These are in stark contrast with the broad and P Cygni profiles, observed in Type Ia/b/c and Type II-P SNe, associated with optically thick line formation in an expanding medium. As shown in the preceding sections, our modelling approach allows us to reproduce this hybrid morphology of a narrow-line core and extended line wings, as illustrated more clearly in our fit to the Hα line profile on 1994 September 1 (Fig. 11).

In Type IIn's, the narrow-line core has been interpreted as line emission from a slowly expanding region. C04 argue that the lack of SN features in the optical spectrum of SN 1994W is in support of the presence of an *optically thick* CDS, whose velocity is of the order of $\sim$4000 km s^{-1}. The narrow-line core flux then stems from the region between the CDS and the outer slowly moving CS shell. The broad wings, according to C04, may stem from various mechanisms/regions. Turbulent, clumpy and fast moving material above the CDS and underneath the outer shell may contribute. Radiation driving may also cause some acceleration of the material just above the CDS, which could then be the origin of some line broadening.

C04 also argue for multiple scattering of line photons by electrons in an optically thick CS envelope. Such non-coherent electron scatterings redistribute line photons in frequency space, and if multiple, can cause a spreading of the line core flux (see below). Because multiple scattering of line photons occurs when the electron-scattering optical depth is large, the presence of such wings has been associated with the presence of an external optically thick CS envelope. The decrease in the strength of these wings as time progresses (Fig. 10)

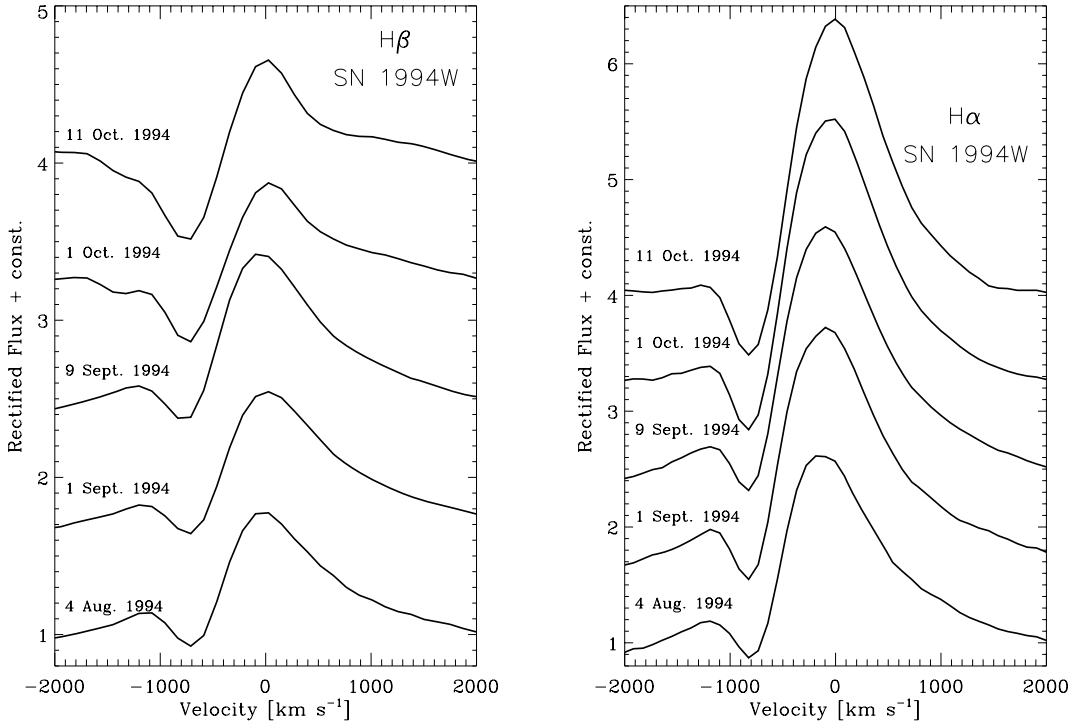

Figure 10. Montage of the evolution (a label gives the date) of the observed Hβ (left-hand panel) and Hα (right-hand panel) line profiles versus Doppler velocity (we correct for a redshift of 1249 km s^{-1}) for SN 1994W (the spectra are normalized to unity at +2000 km s^{-1} and shifted vertically for visibility). Note the extended wings of the narrow-peak Balmer line profiles, with a blue-wing emission contribution that decays with time, by contrast with the strengthening of the red contribution. Note also the velocity blueshift of the emission peak at early times (see Dessart & Hillier 2005a for a physical interpretation), as well as the near-constancy of the velocity location of maximum absorption.

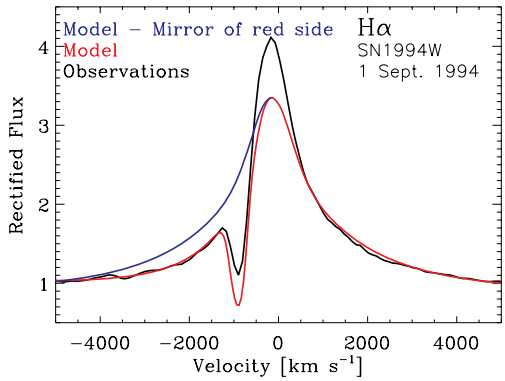

Figure 11. Comparison between the observed (black) and synthetic (red) Hα line profile for 1994 September 1 (see also Fig. 3). Our model of a single formation region for the continuum and lines reproduces the presence of both a narrow-line core (somewhat underestimated) and broad-line wings. Numerous line profiles in the spectrum of SN 1994W share this morphology. To illustrate the stronger red wing flux, we mirror the red part of the Hα profile and draw it in blue on the blue side.

would then follow from the decrease in the shell thickness above the outward-migrating CDS.[2]

Insights into the source of electron scattering can be provided by studying different H lines. For example, a test for the presence of a shell external to the line formation region is that the strength of the electron-scattering wings should be directly proportional to the line flux. Indeed, given the electron-scattering optical depth of the external shell, the number of line photons that end up in the electron-scattering wings of each line should scale with the number of line photons injected at the base of this optically thick layer. In the top left-hand panel of Fig. 12, we show the observed (rectified and scaled) Balmer line profiles on 1994 September 1. Having normalized each peak line flux to unity, it is apparent that the flux in the profile wings increases as we progress up the Balmer series, although for Hδ the rectification may be somewhat in error (there is a background of overlapping lines contributing in the Hδ region). This argues against an external shell as the sole source of electron scattering. However, the observed behaviour can be explained if the regions of line formation and electron scattering overlap.

In the top right-hand panel, we show the corresponding synthetic Balmer line profiles produced with the models described in the previous section. These exhibit the same correlation as the observed profiles – the wings extend ∼3000 km s^{-1} away from line centre, even for the weaker lines in the series, and are strongest for the higher series members. Hence, we do not identify a clear (linear) flux correlation between line core and line wing. By contrast, we find that the synthetic line wing strength scales with the electron-scattering optical depth in the formation region of the corresponding line. In Fig. 13, we plot for Balmer lines (black; the thickness of the line distinguishes the transition), the variation of the quantity $\zeta(R)$ [which corresponds to the emission interior to R in the line through the integral $\int_{R_0}^{R} \zeta(R')\mathrm{d}\log R'$] with respect to the electron-scattering optical depth integrated inwards from the outer grid radius. The relatively weak (strong) line wings of Hα (Hβ) correlate with the relatively low (high) electron-scattering optical

[2] Note that as the optically thick radiating layer migrates outward, the optical thickness of that external shell above it should decrease and eventually vanish. By contrast, line profiles always show narrow-line cores and broad-line wings, over the 80-d period covering the bright phase of the SN.

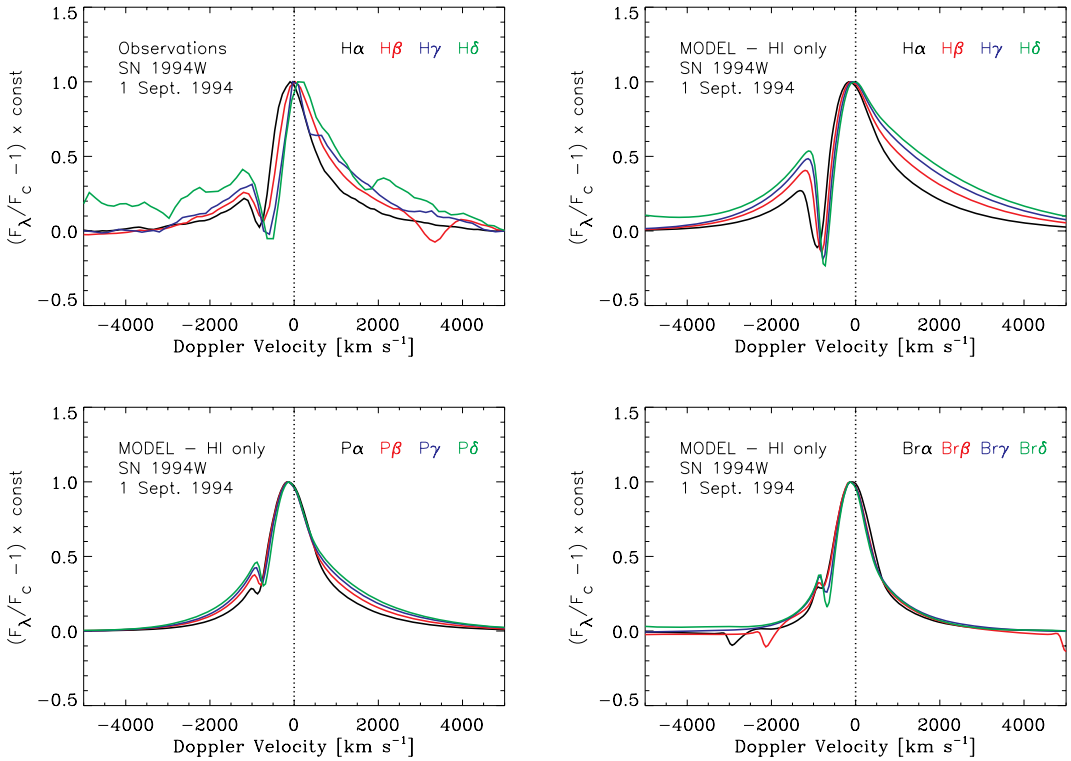

Figure 12. Top panel: observed (left-hand panel) and theoretical (right-hand panel) Balmer line profiles versus Doppler velocity for the first four terms of the series (α: black; β: red; γ: blue and δ: green). For a better comparison, we use the same ordinate range for all panels. We also rectify the spectra and normalize to the peak flux for the corresponding line. Bottom panel: same as top right-hand panel, but this time for the Paschen (bottom left-hand panel) and Brackett (bottom right-hand panel) series. For this illustration, we use the model for the observations of SN 1994W on 1994 September 01, as shown in Fig. 3, but include only the bound–bound transitions of hydrogen (among the first 30 atomic levels). Note how the flux in the line-profile wings gets relatively stronger compared to the peak value as we move up the Balmer series, from Hα to Hδ. We find that electron-scattering wings are stronger for lines that form at higher optical depth (see Fig. 13). If the profile wings were due to an *external* scattering layer, the flux in the profile wings would instead scale linearly with the line flux. Note that the blueshifted absorption at $\sim -3000\,\mathrm{km\,s^{-1}}$ of Brα and at $\sim -2000\,\mathrm{km\,s^{-1}}$ of Brβ (right panel) is due to H I 4.0198 μm and H I 2.6119 μm, respectively.

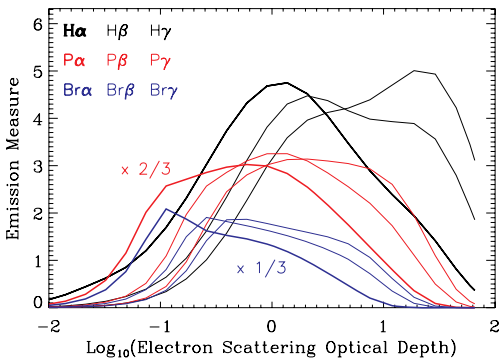

Figure 13. Variation of the emission ζ (Hillier 1987) versus the log of the electron-scattering optical depth for Balmer (black; scaling of unity), Paschen (red; scaling of 2/3) and Brackett (blue; scaling of 1/3) lines for the model shown in Fig. 3. We draw higher series members with thinner lines. The quantity $\zeta(R)$ relates to the total emission interior to R in the line through the integral $\int_{R_0}^{R} \zeta(R')\mathrm{d}\log R'$. $\zeta(R_{\rm Max})$ is the total emission in the line. Note how the site of emission resides deeper in, i.e. at higher optical depth, for higher energy transitions in each series. There appears to be an increasing outward shift from the Balmer to the Paschen and to the Brackett series. In our synthetic spectra, electron-scattering effects are stronger for lines that form deeper in, as observed, and are internal to the photospheric region.

depth in the formation region of the line. In this plot, the situation is most severe for Hγ, which forms deepest. Hence, despite the large Hα flux, the wing flux in both the blue and the red is relatively weaker than in the other lines.

For completeness, we have also included in the bottom panels the predictions for the Paschen and Brackett series. The enhanced scattered flux for high series members is also seen in the Paschen series, but is not so obvious in the Brackett series. This is a key result – Brα has a higher optical depth and forms further out in the envelope than does Hα, and thus exhibits much less obvious electron-scattering wings. Observations of Paschen and Brackett lines would help to provide key information as to the nature of the broad wings. If the layer is external, the fraction of flux in the line wings relative to the line core will be similar for the Balmer and Brackett series, whereas if the electron-scattering layer overlaps the line formation region the fraction of line flux in the line wings will be greatest for the Balmer series. In addition, if a significant fraction of the broad wings arise from intrinsic emission by a fast moving shell/envelope, one would anticipate that the broad wings should be easily discernible in Brα.

To conclude, we find that the strength of the Balmer line profile wings correlates with the electron-scattering optical depth in the corresponding line formation region, the lines forming at greater depths having relatively stronger flux in their wings. In our approach, the broad-line wings are thus formed within the photosphere rather than

caused by an external optically thick shell.[3] In addition, and unlike C04, we find no need for an extra emission source to contribute to the strength of the broad wings.

6.2 Electron scattering theory

In expanding media, electron scattering introduces a systematic redshift of line photons in the observer's frame. This is particularly evident in strong spectral lines observed in SNe and hot star spectra. However, to the steep density fall-off in SN ejecta corresponds a steep drop-off in the electron-scattering optical depth, so that, generally, only a little velocity contrast exists between the emission site of a line photon and the location where it is scattered by a free electron. Free streaming of such line photons prevails soon above the photosphere. The extent of the red-wing electron scattering in SN spectral lines is therefore modest, at least in comparison with what is seen in hot star winds and their characteristic $1/R^2$ density distribution.

A second effect, present even in a medium that is globally at rest, is caused by the relatively large thermal velocity ($V_{\rm th,e} = 550\sqrt{T/10^4}\,{\rm km\,s^{-1}}$) of free electrons, even at moderate temperatures. Scattering with free electrons will lead to appreciable Doppler shifts of line photons relative to the narrow intrinsic width of the line which is typically a few ${\rm km\,s^{-1}}$ (for an ion with atomic weight A, $V_{\rm Dop} = 12(T/A10^4)\,{\rm km\,s^{-1}}$). Upon scattering out of the line core, the photon may be redistributed in frequency into the line wing where the line optical depth is lower, and thus escape entirely from the line. It is then subject to the electron-scattering opacity which prevents it from free streaming to infinity; the photon may experience multiple scatterings with free electrons (with blueshifts/redshifts) before escaping. The frequency shifts may add or cancel but the cumulative statistical effect will lead to an appreciable flux at many electron Doppler widths from line centre, the more so for larger electron-scattering optical depth at the emission site of the photon.

In fast moving SN ejecta, thermal motions are small relative to the expansion velocity; thus, the influence on the observed line profiles of incoherent scattering due to the electron thermal motions is small. However, in slower moving SN ejecta, the frequency shifts due to the thermal motions of the electrons dominate over that due to expansion, and strong red and blue wings are observed. Lines forming deeper in the photosphere, at higher electron-scattering optical depth, show the strongest wing to peak flux ratio, as observed. Here, these numerous electron-scattering events occur internally to the photosphere, rather than in an outer optically thick shell.

In our SN models for SN 1994W, two important effects were observed – the profile shape and to a lesser extent the EW, were strongly dependent on the number of electron-scattering iterations that were performed. To understand this finding, we first need to explain the computational procedure used to compute the line profiles.

To compute the line profiles, we first solve for the atmospheric structure and level populations. These are then used by a separate program, CMF_FLUX (Busche & Hillier 2005), to compute the observed spectrum. For the first iteration, coherent scattering in the comoving frame is assumed. This assumption 'conserves' scattered line photons and allows for redistribution effects due to the expansion of the SN envelope. Using the newly computed mean intensity J, we now allow for the effects of frequency redistribution by electron scattering using the technique of Rybicki & Hummer (1994), and recompute the mean intensity in the comoving frame. To allow for the effects multiple scattering has on the frequency redistribution of line photons, it is necessary to iterate. For fast moving SNe, two iterations are generally sufficient, but for the slow moving SNe, we sometimes had to perform 10 to 20 iterations to get converged line profiles. For accurate calculations, the same Doppler width should be used for both the line-source function and the line profile calculations (Fig. 14). However, for normal SNe changes in the adopted Doppler width have only a minor (and well understood) effect on the line profile.

To further assist in understanding the observed behaviour we also need to consider the relevant scales for both line formation and electron scattering. Since we have a power law density distribution, with exponent n, the characteristic length-scale for electron scattering is $\sim R/(n-1)$. A characteristic scale over which a photon interacts with a line in an expanding medium is the Sobolev length (Sobolev 1960) defined by

$$L_{\rm SOB} = V_{\rm th,eff}/|{\rm d}V/{\rm d}R|, \tag{1}$$

where

$$V_{\rm th,eff} = \sqrt{V_{\rm th,i}^2 + V_{\rm turb}^2} \tag{2}$$

is the effective ion thermal velocity, $V_{\rm th,i}$ is the ion thermal velocity and $V_{\rm turb}$ is a microturbulent velocity that accounts for small-scale turbulent motions. The Sobolev length gives the radial scale over which the velocity changes by $V_{\rm th,eff}$. In other words, it is the approximate size of the resonance zone in which a photon is trapped in a line. In our simulations, we typically adopt $V_{\rm turb} = 50\,{\rm km\,s^{-1}}$, which spreads the line over a broader frequency range than that given by its intrinsic width of a few ${\rm km\,s^{-1}}$.

In the SN context, we have $L_{\rm SOB}/R_{\rm phot} \approx V_{\rm th,eff}/\beta V_{\rm phot}$. The Sobolev length may thus vary through changes in the velocity gradient (controlled by the parameter β) or the ejecta velocity (controlled by $V_{\rm phot}$).[4] In the Type II-P SN 1999em after a few weeks, $V_{\rm phot}$ is of the order of $\sim$4000 ${\rm km\,s^{-1}}$ compared to $\sim$800 ${\rm km\,s^{-1}}$ in SN 1994W. Normalized to $R_{\rm phot}$ and assuming homologous expansion ($\beta = 1$), $L_{\rm SOB}$ is five times larger in SN 1994W compared to SN 1999em.

For SN1994W, $L_{\rm SOB}/R_{\rm phot} = 50/800 = 1/16$ which is only slightly smaller than the electron-scattering scalelength. As this path length is comparable to the electron-scattering scaleheight, there is a significant probability that a photon will be scattered by an electron within the resonance zone. Further, this can facilitate the escape of line photons as the scattering can effectively 'shift' the photon out of the resonance zone by altering its frequency. As we increase $L_{\rm SOB}$, and assuming a fixed line source function, more photons will be incoherently scattered by electrons in the resonance zone. As most of these photons would normally be destroyed,

[3] Another effect could have arisen from the alternate decay channels into transitions that have a lower optical depth. For Hα, there is no alternate decay route for the upper state but to go into $n = 2$. An Hβ photon can yield a couple of Pα–Hα photons. For Hγ, there are more options with Pβ–Hα, Brα–Hβ or Brα–Pα–Hα. The potential escape allowed through a non-coherent electron scattering for Hα could thus be more important compared to higher transitions that have alternate decay routes. If this effect prevailed, the flux in the electron-scattering wings of Hα would be stronger relative to higher transitions in the series, and this is not supported by observations.

[4] The Sobolev length, in general, varies with direction of photon travel, and for photons travelling perpendicular to the radius vector it is always $RV_{\rm th,eff}/V$, independent of the velocity gradient. For simplicity, we retain the formulation above but stress that the average Sobolev length has a much weaker dependence on β than does the radial Sobolev length.

more photons will escape and the line EW will increase. Moreover, since these photons can be subsequently scattered elsewhere, it is necessary to run many iterations to follow their redistribution in frequency space. Because the line EW depends on the adopted Doppler width (and hence the Sobolev length), the line source function should be computed using the same Doppler width.[5]

A critical characteristic of Type IIn SNe compared with more normal Type II SNe is their small photospheric velocity, which leads to both a larger Sobolev length and a larger ratio of $V_{\rm th,eff}/V_{\rm phot}$. Both effects facilitate the appearance of broad wings. The larger Sobolev length facilitates the escape of line photons by electron scattering, even from locations where line photons might not normally escape, and potentially at depths where the electron-scattering optical depth is still significant. The larger ratio $V_{\rm th,eff}/V_{\rm phot}$ makes the incoherent wings due to the thermal motions of the electrons more apparent relative to the observed line width as set by the SN expansion velocity.

We now illustrate these two effects. In Fig. 15, we show a comparison between synthetic Hα line profiles obtained with the model used to fit observations on 1994 October 11, but differing in the adopted values of the base velocity V_0 (the ratio $V_{\rm phot}/V_0$ is the same in all models; $\beta = 1$ in all cases). Increasing V_0 yields broader line cores, the red wing becomes stronger than the blue wing, and the profile looks increasingly asymmetric. Hence, by merely decreasing V_0 from 1500 km s^{-1} to 150 km s^{-1}, we go from a broad P Cygni profile typical for a Type II-P SN to a symmetric line profile with a narrow-line core and broad-wings typical for a Type IIn SN.

In Fig. 16, we show models with different velocity distributions but varying the exponent β entering the velocity law. Recall that reducing β first reduces the maximum velocity, but it also increases the Sobolev length. Hence, by reducing β one can reduce the redistribution of line photons to the red associated with expansion, and increase the importance of electron scattering as a means of escape for line photons. All three models shown in Fig. 16 yield a quasi-symmetric profile that extends from line centre out to $\pm$3000 km s^{-1}, although the maximum expansion velocity in the ejecta varies from 4000, to 1364, and 1123 km s^{-1}, as we reduce β from 1, to 0.2, and 0.01, respectively. A non-coherent electron scattering is thus the primary line broadening mechanism, so that, paradoxically, the broad-line wings testify for slow rather than fast expansion. For smaller β, the blue-wing emission strengthens and arises exclusively from redistribution to the blue of photons in the line core. This occurs at the expense of the line core flux, which indeed decreases correspondingly.

Another element of interest in the observed Balmer line profiles shown in the top left-hand panel of Fig. 12 is the location of the P Cygni profile dip, which ranges from -900 km s^{-1} for Hα to -500 km s^{-1} for Hδ on 1994 September 1. The velocity shift of this absorption component is well reproduced by our synthetic line profiles, as shown in the top right-hand panel of Fig. 12. In our modelling approach, which assumes a linearly increasing velocity with radius, the more optically thick line forms further out, in a region that moves faster, thereby showing a P Cygni profile absorption further to the blue from line centre. In other words, the velocity shift of the absorption minimum amongst the Balmer lines suggests the velocity increases outwards from the photosphere. This is different from the narrow absorption (and sometimes associated narrow emission) that is sometimes seen on top of the strong and broad Hα line profile and that is associated with the CS material exclusively (see Kotak et al. 2004 for the Type Ia SN 2002ic, Smith et al. 2007 for SN 2006gy and Salamanca et al. 2002 for SN 1997eg).

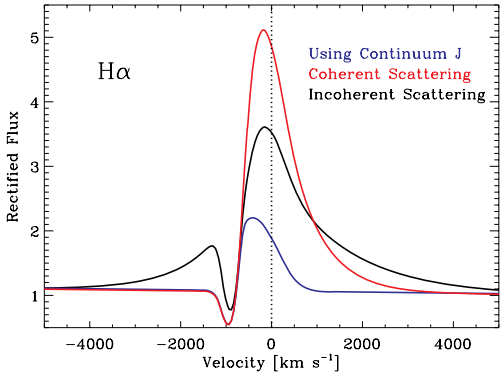

Figure 14. Comparison between the synthetic Hα line profile obtained assuming incoherent (black) or coherent (red) electron scattering in the comoving frame. In blue, we show the effect of using the continuum (rather than the line) mean intensity when computing the electron-scattering source function, which shows that a large fraction of line photons suffer at least one scattering with free electrons as they escape from their emitting region. For this illustration, we use the same model that fits the observations of SN 1994W on 1994 September 1, whose characteristics are given in Table 1.

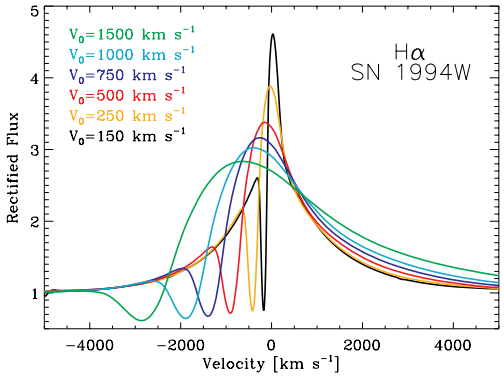

Figure 15. Comparison between synthetic Hα line profiles versus Doppler velocity obtained with the model used to fit observations on 1994 October 11, but differing in the adopted values of the base velocity V_0 [the velocity law is of the form $v(R) = V_0(R/R_0)^\beta$]. By decreasing V_0 from 1500 to 150 km s^{-1}, we go from a broad P-Cygni profile typical for a Type II-P SN to a symmetric line profile with a narrow-line core and broad wings typical for a Type IIn SN. (See the text for discussion.)

7 DISCUSSION AND CONCLUSIONS

In this work, we have performed a quantitative spectroscopic analysis of the interacting Type IIn SN 1994W, an unusual Type II event

[5] All synthetic spectra shown here are computed with a value of 10 km s^{-1} for the turbulent velocity. Note that to limit the computation time, this choice only applies when computing the emergent spectrum from a formal solution of the transfer equation. When solving for the full radiation transport problem including level populations, we assume a turbulent velocity of 50 km s^{-1}, and generally assume that electron scattering is coherent in the comoving frame (i.e. we ignore redistribution effects due to the thermal motions of the electrons), so as to allow the linearization of the electron-scattering source function (see Hillier & Miller 1998 for the details). Tests we performed show that there is a weak sensitivity of the level populations and the emergent radiation field to variations in the turbulent velocity from 10 to 50 km s^{-1} – the choice of 50 km s^{-1} minimizes computational effort and is numerically advantageous.

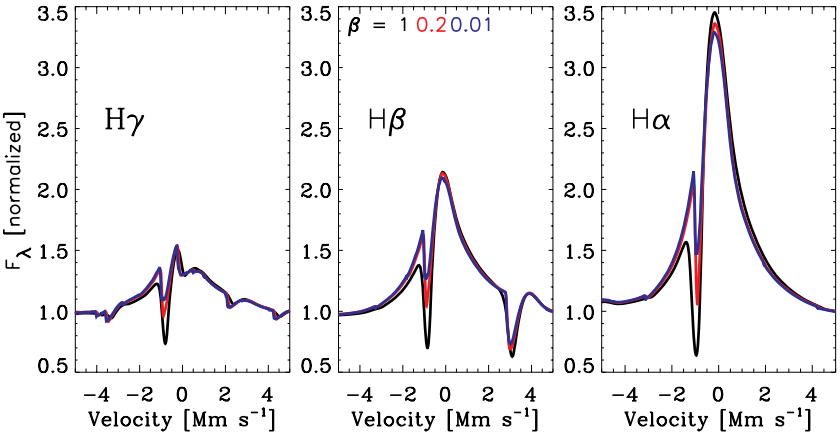

Figure 16. Left-hand panel: variation of the Hγ line profile computed for different assumptions on the ejecta velocity distribution, i.e. characterized by $v(R) = V_0(R/R_0)^\beta$, with β equal to 1 (black; $V_{\rm Max} = 4000\,{\rm km\,s^{-1}}$), 0.2 (red; $V_{\rm Max} = 1364\,{\rm km\,s^{-1}}$) and 0.01 (blue; $V_{\rm Max} = 1123\,{\rm km\,s^{-1}}$). Middle panel: same as the left-hand panel, but this time for Hβ. Right-hand panel: same as left-hand panel, but this time for Hα. The reference model with $\beta = 1$ is used to fit observations of SN 1994W on 1994 September 1 (see Fig. 3 and Table 1). For the latter two models, the base velocity is adjusted so that the photospheric velocity is within 10 per cent of $830\,{\rm km\,s^{-1}}$, thence, producing a similar line core width. Expansion causes little red-wing broadening since these three models, which differ so much in maximum ejecta velocity $V_{\rm Max}$, show a similar redwing extent. Effects of non-coherent and multiple scattering by thermal electrons are the primary cause of the extended wings. Note how the profile becomes more symmetric, i.e. shows a stronger blue electron-scattering wing, as β (or the velocity gradient, which controls the escape probability of a photon trapped in the line) is reduced.

that exhibited narrow-line cores with broad-line wings in the optical, was unusually luminous, showed erratic spectral behaviour prior to peak brightness and synthesized an extremely low amount of ^{56}Ni. Our study covers specifically from 10–20 d prior to peak until 50 d afterwards, and makes use of a radiative-transfer modelling approach that is one-dimensional and steady-state, assumes a (steep) power-law density distribution and a linear velocity law. Importantly, it incorporates non-LTE effects and accurately treats the electron-scattering source function.

During the brightening phase, also characterized by a strong spectral variability, we suspect the presence of multiple radiating regions, split between an optically thick layer contributing to the bulk of the optical light, and shocked (and perhaps clumpy) material above contributing a smaller and rapidly variable fraction. This fraction is subdominant in the optical but could be much larger in the ultraviolet (UV) and X-ray ranges. Because this outer, low-density, material has been shocked to high temperatures, it is optically thin and, thus, radiatively less efficient (see Fransson et al. 1996). Such a dichotomy is also supported by the *simultaneous* presence of optical spectral features testifying for both relatively low- and high-ionization conditions (i.e. Fe II and He I). Our models during this brightening phase are mostly exploratory, but suggestive of a complex interaction configuration. Observations over a broad spectral band, and extending into at least the near UV, are crucial for understanding these earlier phases.

During the monotonic and slow fading phase, our fits are by contrast very satisfactory. We find that the bolometric light must emerge entirely from a single hydrogen-rich optically thick layer moving at a near-constant velocity of $\sim$800 km s^{-1}. This photosphere recedes in both mass and radius with time, its extent shrinking from 4.3×10^{15} at peak to 2.3×10^{15} cm 50 d later, while cooling modestly from $\sim$7300 to $\sim$6300 K over that same period. As in Type II-P SNe, we find that the photosphere is slaved to the region of full ionization, which, as the material expands and radiates, can only shrink. The steep fading 50 d after the peak is, thus, naturally associated with the emitting material becoming completely optically thin. The near-constant photospheric velocity of $\sim$800 km s^{-1}, for an extended period (over 60 d), places strong constraints on dynamical models.

The above parameters result from the radiative transfer modelling of the spectroscopic and photometric evolution of SN 1994W, and represent what is required to reproduce observations. These properties should therefore be matched by any radiation hydrodynamics modelling of SN 1994W – they represent an important guide. In the context of an interaction between the inner and outer ejecta, this photosphere would likely reside somewhere between the reverse shock (located in the inner ejecta) and the forward shock (located in the outer ejecta). The inferred photospheric velocity cannot be associated with CSM alone since a large overdensity and full ionization are required to create this optically thick layer, a condition that is met only between the reverse and forward shocks (it cannot reside inside of the reverse shock since this would be the inner fast ejecta and all emission profiles would appear much broader than they do).

As this was a preliminary study, each epoch was modelled independently – we did not attempt to get consistency in the parameters between different dates (i.e. the photospheric density at day 90 is lower than what would be inferred by a power-law extrapolation of the photospheric density at day 50). Whether a consistent density/velocity set could be obtained will require a more consistent approach, possibly in conjunction with dynamical modelling. The results of such an investigation would provide crucial constraints on the dynamical model of the emitting region.

By contrast with C04, we do not find that the CDS represents such a key landmark for the understanding of the light coming from SN 1994W. The CDS may be optically thick at early times, but it must be optically thin after the peak to explain the fading phase of the SN, which would otherwise be a brightening phase given the small photospheric temperature decrease. A corollary is that the steep fading at late times corresponds to the onset of the nebular phase rather than to the CDS leaving the external shell.

We reproduce successfully the narrow-core broad-wing line profile morphology in the optical spectra of SN 1994W at all epochs, thus downplaying the alleged role of an optically thick external

shell in causing this profile shape. Instead, we find that this hybrid morphology results from the conditions at the photosphere alone. Indeed, we argue that the small photospheric velocity of SN 1994W at all times recorded makes electron scattering a key escape mechanism for line photons. The associated frequency kicks redistribute photons from the optically thick line cores where they are trapped into the more optically thin line wings, from where they can escape after several scatterings with free electrons. The resulting flux in the wings increases at the expense of the flux in the line core. Paradoxically, the slower the photospheric velocity, the broader and more evident the line wings, which thus reflect the slow rather than the fast expansion of the flow. As C04, we find that the effect is more pronounced for high electron-scattering optical depth, but we associate this effect with the photosphere exclusively, where both lines and continuum form, rather than with an external shell. C04 estimated the properties of the external shell based on estimates of its electron-scattering optical depth through the effect on line profiles. This needs revision since the observed narrow-line cores and broad-line wings can be understood from multiple scattering internal to the photosphere. Indeed, we can explain the entire optical spectrum by a single emitting region. To avoid any misunderstanding, let us stress again. We are not proposing that there is no external shell. Rather, we find that the multiple electron-scattering events at the origin of the broad-line wings do not occur in the external shell, but are instead internal to that localized, optically thick, layer where most photons are produced and which, we demonstrated, exist unambiguously.

Let us now *speculate* on what may be at the origin of the SN 1994W event. This speculation is motivated by two recent observations that show that Type IIn SNe are associated with widely different progenitors. First, objects like the Type IIn SN 2006gy are associated with a large bolometric luminosity (a rate in excess of $10^{10}\,L_\odot$ sustained for months), a large kinetic energy (there is interaction, hence deceleration, but still the line profiles are much broader than for SN 1994W) and a large amount of mass in both the inner and outer ejecta that interact (because the ejecta remain optically thick for months). These objects must be associated with very massive stars, losing considerable amounts of mass in at least two events, and exploding with a prodigious energy which seems to require either gravitational collapse or thermonuclear burning. Secondly, the Type IIn SN 2008S progenitor is identified on pre-explosion images as a star of $\sim$10 $M_\odot$ (Prieto et al. 2008). That two SNe with the same type be associated with progenitors of such different properties suggest that such interactions can occur in a wide variety of circumstances. Further, the observations (e.g. SN 2008S; Prieto et al. 2008) show that SN IIn are not necessarily associated with LBVs. Note that stars in the mass range 8–10 $M_\odot$ are considerably more numerous than high-mass progenitors at the origin of SN 2006gy-like events. Moreover, they do not build degenerate Fe cores, but ONeMg ones.

In the speculative statements we present below, we wish to raise the issue that (i) given an interaction has to occur to explain the combination of large photospheric radii and small expansion velocities (inferred from line profile widths) and (ii) given that Type II SNe have typically 100 times more kinetic energy than radiant energy (1 B compared to 0.01 B; 1B $\equiv 10^{51}$ erg), conversion efficiencies of a few to a few tens of per cent from kinetic to internal energy can satisfy the energetics of most Type IIn SNe. With such a huge kinetic energy reservoir, any modest conversion to internal energy can give rise to SN-like displays. And indeed, the fact that statistically, the brightest SNe known are of Type IIn is compelling. Hence, the kinetic energy and mass budget, the conversion efficiency from kinetic to internal energy and the expected variety of CS material configurations, offer a natural way to explain both the brightness and the diversity of Type IIn SNe (see Introduction for a short synopsis of this diversity). Our speculation, now, is that one may not systematically need 1 B of kinetic energy to power a Type IIn SN bolometric display.

Turning to SN 1994W, and adopting a representative luminosity of $2 \times 10^9\,L_\odot$ over a 100-day period, the time-integrated bolometric light for SN 1994W is $E_{\rm rad} \approx 0.066$ B. With a conversion efficiency of 30 per cent (which is at the upper end of what Chevalier (1983) proposes for driven waves; variations of a few per cent can be accommodated given the speculative level meant in the present discussion), this would require a kinetic energy of $E_{\rm kin} \approx 0.2$ B, which can be matched by, for example, a $2\,M_\odot$ shell moving at 3000 km s^{-1}. One can try different combinations of mass and velocity, but the point here is that this does not represent so much energy. This may not be what happens in SN 19994W, but it demonstrates that modest kinetic energies, i.e. less than standard core-collapse SN explosion energies, do not violate any of the energetics to power the bolometric displays like that of SN 1994W. Whether they do in practice needs to be demonstrated. In this context, it seems that a shell–shell interaction could explain, in principle, the radiation budget of SN 1994W, and that a powerful core-collapse SN explosion may not be needed. Additionally, the absence of core collapse and potential nickel production would satisfy the very low nickel yields inferred for this SN, a record low of 0.0026–0.015 $M_\odot$ (SCL). It can also explain more easily the absence of broad lines at all times. The mechanism for the ejection of the second shell would also be the same one as for the first shell, but the second ejection would have to expand faster to catch up the first. We note that no massive star is known to have a radius larger than 10^{14} cm (red supergiant, see Levesque et al. 2005), so there should be ample time to detect and thoroughly observe the expansion of the inner shell prior to interaction, in fact about $100/V_3$ d (assuming constant velocity expansion), and determine its properties. Note, however, that none of these observations alone is sufficient to rule out a core collapse, but they do suggest that other mechanisms should also be examined. For example, a low Ni yield, by itself, does not rule out a core-collapse SN. Recent theoretical simulations of 8–10 $M_\odot$ stars indicate that the resulting SN can give low Ni yields ($<$0.015 $M_\odot$) (e.g. Kitaura, Janka & Hillebrandt 2006). SN 2005cs is regarded as a low-luminosity SN, is considered to have arisen from a low-mass progenitor (e.g. Eldridge, Mattila & Smartt 2007) and had a low Ni yield of $\sim$0.01 $M_\odot$ (Pastorello et al. 2006; Tsvetkov et al. 2006). Fall-back may also truncate the inner, nickel-rich ejecta (Woosley & Timmes 1996), but the quantitative aspects of this process are uncertain, and one may wonder why these Type IIn SNe, whose properties are really set by an external interaction, would also have experienced significant fall back.

C04 inferred the presence of a 0.4 $M_\odot$ CS envelope, while we know that core-collapse SN ejecta have at least 6 $M_\odot$, typically endowed with 1 B kinetic energy.[6] Given this unequal mass configuration, it is unlikely that the SN ejecta could be decelerated throughout to velocities below 1000 km s^{-1}. A more favourable configuration for deceleration, supported by the narrow lines at all times, is for two shells of comparable mass. The mechanism causing the shell ejections is unknown, but may be related to pulsations or nuclear

[6] Only stars more massive than 8 $M_\odot$ on the main sequence undergo core collapse, so, leaving aside 2 $M_\odot$ for the neutron star and fall-back material leaves us with at least 6 $M_\odot$. More generic values may be 10–15 $M_\odot$.

flashes in the last stages of core burning. For example, within ∼2 yr of core collapse, 20 $M_\odot$ main-sequence stars go through a ∼1.5 yr long oxygen core-burning phase: instabilities associated with that phase that led to an explosive shell ejection would provide a reproducible time delay before collapse and an attractive mechanism at the origin of some Type IIn SNe like 1994W. Woosley et al. (2007) have invoked the same mechanism, the collision between ejected shells, to explain the extremely luminous supernova SN 2006gy. In the model of Woosley et al. (2007), pair-instability pulsations in massive stars (e.g. $M \gtrsim 110\,M_\odot$) eject multiple shells which later collide.

CS envelopes with kinetic energies with >0.01 B erg are known. In the 1840s, Eta Carinae underwent a major outburst ejecting over 10 $M_\odot$ of material at a velocity of 650 km s^{-1}, with kinetic energy ≳0.04 B (Smith et al. 2003). Unfortunately, the duration of the ejection event is not well constrained, and there is no consensus as to the cause of the event. More interestingly, Eta Carinae underwent a second eruption, most likely in the 1890s, although the event was much less significant (0.1 $M_\odot$, $V \sim 200$ km s^{-1}, 10^{-4} B; Smith et al. 2003). While the dynamics and kinematics do not satisfy the requirements for a bright CS interaction, they are in the least suggestive that such an interaction might occur. A potential issue with shell ejections from LBVs and similar stars is that the ejection velocities tend to scale with the escape speed. For SN 1994W, it is likely the second shell needed speeds of the order of 1500 km s^{-1}, or larger. A direct corollary of the shell interaction scenario is that the progenitor star would not be destroyed (although it might be difficult to detect in the optical if dust formed), and this offers a direct means of distinguishing between the core-collapse and multiple shell-ejection scenarios. Similarly, direct confirmation of Ni/Co decay could be used to distinguish between the two models.

Type IIn SNe gather a very heterogeneous group and our findings should not be applied blindly to the other Type IIn SNe. In some cases (e.g SN 1988Z, Stathakis & Sadler 1991; Turatto et al. 1993; van Dyk et al. 1993; Chugai & Danziger 1994), it is readily apparent that core-collapse SN ejecta, interacting with CS matter, can explain the observed spectral variations. To make further progress, detailed radiation hydrodynamics of the interaction and detailed radiative transfer calculations of the emergent spectra need to be performed in partnership, and for a wide range of configurations. Allowance for time-dependent effects and departures from sphericity may also be needed. Observations in the blue (as far to the UV as possible), red and near-infrared would provide critical constraints on the models. As a key probe of shocks, X-ray observations are crucial. Finally, public availability of all observational data would help to reveal fully the diversity of Type IIn spectra and light curves, thereby helping understand this challenging group of SNe.

ACKNOWLEDGMENTS

We thank Adam Burrows, Rubina Kotak, Jeremiah Murphy and Steve Smartt for discussion, Robert Cumming for providing the SN 1994W spectroscopic data used here, Nikolai Chugai for his comments and Stéphane Blondin for a thorough reading of a draft of this paper and his suggestions. LD acknowledges support for this work from the Scientific Discovery through Advanced Computing (SciDAC) program of the DOE, under grant numbers DOE-FC02-01ER41184 and DOE-FC02-06ER41452, and the NSF under grant number AST-0504947.

REFERENCES

Anupama G. C., Sivarani T., Pandey G., 2001, A&A, 367, 506
Aretxaga I., Benetti S., Terlevich R. J., Fabian A. C., Cappellaro E., Turatto M., della Valle M., 1999, MNRAS, 309, 343
Bautista M. A., Pradhan A. K., 1997, A&AS, 126, 365
Becker S. R., Butler K., 1995, A&A, 301, 187
Benetti S., Cappellaro E., Turatto M., Taubenberger S., Harutyunyan A., Valenti S., 2006, ApJ, 653, L129
Bowen D. V., Roth K. C., Meyer D. M., Blades J. C., 2000, ApJ, 536, 225
Brown P. J. et al., 2007, ApJ, 659, 1488
Busche J. R., Hillier D. J., 2005, AJ, 129, 454
Butler K., Mendoza C., Zeippen C. J., 1993, J. Phys. B: At. Mol. Phy., 26, 4409
Cardelli J. A., Clayton G. C., Mathis J. S., 1989, ApJ, 345, 245
Castor J. I., Abbott D. C., Klein R. I., 1975, ApJ, 195, 157
Chandra P., Ray A., Schlegel E. M., Sutaria F. K., Pietsch W., 2005, ApJ, 629, 933
Chevalier R., 1982, ApJ, 258, 790
Chevalier R., 1983, ApJ, 272, 765
Chevalier R. A., Fransson C., 1994, ApJ, 420, 268
Chevalier R. A., Fransson C., 2003, in Weiler K., ed., Supernovae and Gamma-Ray Bursters, Lecture Notes Phys. Vol. 598. Springer, Berlin, p. 171
Chugai N. N., 2001, MNRAS, 326, 1448
Chugai N. N., Chevalier R. A., 2007, ApJ, 657, 378
Chugai N. N., Danziger I. J., 1994, MNRAS, 268, 173
Chugai N. N., Danziger I. J., 2003, Astron. Lett., 29, 649
Chugai N. N., Yungelson L. R., 2004, Astron. Lett., 30, 65
Chugai N. N., Blinnikov S. I., Fassia A., Lundqvist P., Meikle W. P. S., Sorokina E. I., 2002, MNRAS, 330, 473
Chugai N. N. et al., 2004a, MNRAS, 352, 1213 (C04)
Chugai N. N., Chevalier R. A., Lundqvist P., 2004b, MNRAS, 355, 627
Davidson K., Humphreys R. M., 1997, ARA&A, 35, 1
Deng J. et al., 2004, ApJ, 605, L37
Dessart L., Hillier D. J., 2005a, A&A, 437, 667
Dessart L., Hillier D. J., 2005b, A&A, 439, 671
Dessart L., Hillier D. J., 2006, A&A, 447, 691
Dessart L., Hillier D. J., 2008, MNRAS, 383, 57
Dessart L. et al., 2008, ApJ, 675, 644
Eldridge J. J., Mattila S., Smartt S. J., 2007, MNRAS, 376, L52
Fabian A. C., Terlevich R., 1996, MNRAS, 280, L5
Fassia A. et al., 2000, MNRAS, 318, 1093
Fassia A. et al., 2001, MNRAS, 325, 907
Foley R. J., Smith N., Ganeshalingam M., Li W., Chornock R., Filippenko A. V., 2007, ApJ, 657, L105
Fox D. W. et al., 2000, MNRAS, 319, 1154
Fransson C., Lundqvist P., Chevalier R. A., 1996, ApJ, 461, 993
Fransson C. et al., 2002, ApJ, 572, 350
Fransson C. et al., 2005, ApJ, 622, 991
Fuhr J. R., Martin G. A., Wiese W. L., 1988, Atomic Transition Probabilities. Am. Inst. Phys., New York
Gao Y., Solomon P. M., 2004, ApJS, 153, 62
Gerardy C. L., Fesen R. A., Höflich P., Wheeler J. C., 2000, AJ, 119, 2968
Hamuy M. et al., 2003, Nat, 424, 651
Han Z., Podsiadlowski P., 2006, MNRAS, 368, 1095
Hillier D. J., 1987, ApJS, 63, 965
Hillier D. J., Miller D. L., 1998, ApJ, 496, 407
Hoffman J. L., Leonard D. C., Chornock R., Filippenko A. V., Barth A. J., Matheson T., 2008, ApJ, 688, 1186
Hummer D. G., Berrington K. A., Eissner W., Pradhan A. K., Saraph H. E., Tully J. A., 1993, A&A, 279, 298
Kingdon J. B., Ferland G. J., 1996, ApJS, 106, 205
Kitaura F. S., Janka H.-T., Hillebrandt W., 2006, A&A, 450, 345
Kotak R., Meikle W. P. S., Adamson A., Leggett S. K., 2004, MNRAS, 354, L13
Kraan-Korteweg R. C., 1986, A&AS, 66, 255

Kurucz R. L., 1988, in Viotti R., Vittone A., Friedjung M., eds, IAU Colloq. 94, Physics of Formation of Fe II lines outside LTE. Astron. Soc. Pac., San Francisco, p. 41
Kurucz R. L., 2002, in Schulz D. R., Krstic P. S., Ownby F., eds, Atomic and Molecular Data and Their Applications, ASP Conf. Ser. Vol. 636. Astron. Soc. Pac., San Francisco, p. 134
Kurucz R. L., Bell B., 1995, Kurucz CD-ROM. Smithsonian Astrophysical Observatory, Cambridge, MA
Lentz E. J. et al., 2001, ApJ, 547, 406
Leonard D. C., Filippenko A. V., Barth A. J., Matheson T., 2000, ApJ, 536, 239
Levesque E. M., Massey P., Olsen K. A. G., Plez B., Josselin E., Maeder A., Meynet G., 2005, ApJ, 628, 973
Liu Q.-Z., Hu J.-Y., Hang H.-R., Qiu Y.-L., Zhu Z.-X., Qiao Q.-Y., 2000, A&AS, 144, 219
Luo D., Pradhan A. K., 1989, J. Phys. B: At. Mol. Phy., 22, 3377
Luo D., Pradhan A. K., Saraph H. E., Storey P. J., Yan Y., 1989, J. Phys. B: At. Mol. Phy., 22, 389
Matheson T., Filippenko A. V., Chornock R., Leonard D. C., Li W., 2000, AJ, 119, 2303
Mendoza C., 1983, IAU Symp., 103, 143
Mendoza C., Eissner W., LeDourneuf M., Zeippen C. J., 1995, J. Phys. B: At. Mol. Phy., 28, 3485
Mucciarelli P., Zampieri L., Turatto A. P. M., Cappellaro E., Benetti S., 2006, Mem. Soc. Astron. Ital. Suppl., 9, 391
Nahar S. N., 1995, A&A, 293, 967
Nahar S. N., 1996, Phys. Rev. A, 53, 1545
Nahar S. N., Pradhan A. K., 1996, A&AS, 119, 509
Neufeld D. A., Dalgarno A., 1987, Phys. Rev. A, 35, 3142
Nussbaumer H., Storey P. J., 1983, A&A, 126, 75
Nussbaumer H., Storey P. J., 1984, A&AS, 56, 293
Ofek E. O. et al., 2007, ApJ, 659, L13
Pastorello A. et al., 2002, MNRAS, 333, 27
Pastorello A. et al., 2006, MNRAS, 370, 1752
Pastorello A. et al., 2007, Nat, 447, 829
Peach G., Saraph H. E., Seaton M. J., 1988, J. Phys. B: At. Mol. Phy., 21, 3669
Pooley D. et al., 2002, ApJ, 572, 932
Pozzo M., Meikle W. P. S., Fassia A., Geballe T., Lundqvist P., Chugai N. N., Sollerman J., 2004, MNRAS, 352, 457
Pozzo M., Meikle W. P. S., Fassia A., Geballe T., Lundqvist P., Chugai N. N., Sollerman J., 2005, in Turatto M., Benetti S., Zampieri L., Shea W., eds, 1604-2004: Supernovae as Cosmological Lighthouses, ASP Conf. Ser. Vol. 342. Astron. Soc. Pac., San Francisco, p. 337
Pradhan A. K., Zhang H. L., Nahar S. N., Romano P., Bautista M. A., 1996, BAAS, 28, 1367
Prieto J. L. et al., 2008, ApJ, 681, L9
Ralchenko Y., Kramida A. E., Reader J., NIST ASD Team 2008. NIST Atomic Spectra Data base (version 3.1.5), http://physics.nist.gov/asd3. National Institute of Standards and Technology, Gaithersburg, MD
Rybicki G. B., Hummer D. G., 1994, A&A, 290, 553
Salamanca I., Terlevich R. J., Tenorio-Tagle G., 2002, MNRAS, 330, 844
Schlegel E. M., 1999, ApJ, 527, L85
Schlegel E. M., Petre R., 2006, ApJ, 646, 378
Seaton M., 1987, J. Phys. B: At. Mol. Phy., 20, 6363
Smith N., 2005, MNRAS, 357, 1330
Smith N., McCray R., 2007, ApJ, 671, L17
Smith N., Gehrz R. D., Hinz P. M., Hoffmann W. F., Hora J. L., Mamajek E. E., Meyer M. R., 2003, ApJ, 125, 1458
Smith N. et al., 2007, ApJ, 666, 1116
Sobolev V. V., 1960, Moving Envelopes of Stars. Harvard Univ. Press, Cambridge
Sollerman J., Cumming R. J., Lundqvist P., 1998, ApJ, 493, 933 (SCL)
Stathakis R. A., Sadler E. M., 1991, MNRAS, 250, 786
Tsvetkov D. Y., 1995, IBVS, 4253, 1
Tsvetkov D. Y., Volnova A. A., Shulga A. P., Korotkiy S. A., Elmhamdi A., Danziger I. J., Ereshko M. V., 2006, A&A, 460, 769
Tully J. A., Seaton M. J., Berrington K. A., 1990, J. Phys. B: At. Mol. Phy., 23, 3811
Turatto M., Cappellaro E., Danziger I. J., Benetti S., Gouiffes C., della Valle M., 1993, MNRAS, 262, 128
van Dyk S. D., Weiler K. W., Sramek R. A., Panagia N., 1993, ApJ, 419, L69
Wang L., Baade D., Höflich P., Wheeler J. C., Kawabata K., Nomoto K., 2004, ApJ, 604, L53
Wiese W. L., Smith M. W., Glennon B. M., 1966, NSRDS-NBS 4. US Department of Commerce, National Buereau of Standards, Washington, DC
Wiese W. L., Smith M. W., Miles B. M., 1969, NSRDS-NBS. US Department of Commerce, National Bureau of Standards, Washington, DC
Williams C. L., Panagia N., Van Dyk S. D., Lacey C. K., Weiler K. W., Sramek R. A., 2002, ApJ, 581, 396
Wood-Vasey W. M., Wang L., Aldering G., 2004, ApJ, 616, 339
Wood-Vasey W. M., Sokoloski J. L., 2006, ApJ, 645, L53
Woosley S. E., Janka T., 2005, Nat. Phys., 1, 147
Woosley S. E., Timmes F. X., 1996, Nucl. Phys. A, 606, 137
Woosley S. E., Blinnikov S., Heger A., 2007, Nat, 450, 390
Zampieri L., Mucciarelli P., Pastorello A., Turatto M., Cappellaro E., Benetti S., 2005, MNRAS, 364, 1419
Zhang H. L., Pradhan A. K., 1995, A&A, 293, 953
Zhang H. L., Pradhan A. K., 1997, A&AS, 126, 373

APPENDIX A

The following tables provide a summary of the spectral lines important for fitting SN 1994W at different dates. Line equivalent widths were computed assuming isolated lines, and using a modified form of the Sobolev approximation. They are meant to provide a guide to the relative importance of various features in the spectrum, and should NOT be used for quantitative analysis. The level name notation is based on the notation of levels in CMFGEN which in turn is based on the notation from NIST (Ralchenko et al. 2008).

Table A1. Excerpt of line list for model used to match observations on 1994 September 01. The full table is available as Supporting Information.

λ (Å)	W_λ (Å)	Species	Transition (upper level – lower level)
3213.3	−1.5	Fe II	$3d^6\ (^5D)\ 4p\ z\,^4D^o_{5/2} - 3d^7\ a\,^4P_{3/2}$
3227.7	−1.6	Fe II	$3d^6\ (^5D)\ 4p\ z\,^4D^o_{7/2} - 3d^7\ a\,^4P_{5/2}$
3662.3	1.2	H I	30 – 2
3663.4	1.4	H I	29 – 2
3664.7	1.5	H I	28 – 2
3666.1	1.7	H I	27 – 2
3667.7	1.9	H I	26 – 2
3669.5	2.2	H I	25 – 2
3671.5	2.4	H I	24 – 2
3673.8	2.6	H I	23 – 2

Table A2. Excerpt of line list for model used to match observations on 1994 September 09. The full table is available as Supporting Information.

λ (Å)	W_λ (Å)	Species	Transition (upper level – lower level)
3210.4	−1.4	Fe II	$3d^6\ (^5D)\ 4p\ z\,^4D^o_{3/2} - 3d^7\ a\,^4P_{1/2}$
3213.3	−2.1	Fe II	$3d^6\ (^5D)\ 4p\ z\,^4D^o_{5/2} - 3d^7\ a\,^4P_{3/2}$
3227.7	−2.2	Fe II	$3d^6\ (^5D)\ 4p\ z\,^4D^o_{7/2} - 3d^7\ a\,^4P_{5/2}$
3408.8	−1.2	Cr II	$3d^4\ (^5D)\ 4p\ z^6D^o_{5/2} - 3d^4\ (^5D)\ 4s\ a\,^4D_{7/2}$
3422.7	−1.0	Cr II	$3d^4\ (^5D)\ 4p\ z\,^4P^o_{3/2} - 3d^4\ (^5D)\ 4s\ a\,^4D_{5/2}$
3442.0	−1.1	Mn II	$3d^5\ (^6S)\ 4p\ z\,^5P^o_3 - 3d^6\ a\,^5D_4$
3514.0	−1.3	Ni II	$3d^8\ (^3F)\ 4p\,^4D^o_{7/2} - 3d^8\ (^3P)\ 4s\,^4P_{5/2}$
3662.3	1.2	H I	30 – 2
3663.4	1.4	H I	29 – 2
3664.7	1.6	H I	28 – 2

Table A3. Excerpt of line list for model used to match observations on 1994 October 01. The full table is available as Supporting Information.

λ (Å)	W_λ (Å)	Species	Transition (upper level – lower level)
3202.5	−3.4	Ti II	$3d^2$ (^{1}D) 4p $y^2F^o_{5/2}$ – $3d^2$ (^{1}D) 4s $a^2D_{3/2}$
3203.4	−1.4	Ti II	$3d^2$ (^{3}F) 4p $z^2F^o_{5/2}$ – $3d^2$ (^{3}F) 4s $a^4F_{3/2}$
3210.4	−5.1	Fe II	$3d^6$ (^{5}D) 4p $z^4D^o_{3/2}$ – $3d^7$ $a^4P_{1/2}$
3211.1	−1.1	Fe II	$3d^6$ (^{3}F2) 4p $x^4D^o_{7/2}$ – $3d^7$ $b^2F_{5/2}$
3212.0	−2.7	Fe II	$3d^6$ (^{3}H) 4p $z^4I^o_{9/2}$ – $3d^6$ (^{3}G) 4s $b^2G_{9/2}$
3213.3	−6.4	Fe II	$3d^6$ (^{5}D) 4p $z^4D^o_{5/2}$ – $3d^7$ $a^4P_{3/2}$
3214.8	−2.0	Ti II	$3d^2$ (^{3}F) 4p $z^2F^o_{7/2}$ – $3d^2$ (^{3}F) 4s $a^4F_{9/2}$
3217.1	−4.1	Ti II	$3d^2$ (^{3}F) 4p $z^4F^o_{9/2}$ – $3d^2$ (^{3}F) 4s $a^4F_{7/2}$
3218.3	−2.4	Ti II	$3d^2$ (^{1}G) 4p $y^2G^o_{7/2}$ – $3d^3$ $a^2H_{9/2}$
3222.8	−4.4	Ti II	$3d^2$ (^{3}F) 4p $z^4F^o_{7/2}$ – $3d^2$ (^{3}F) 4s $a^4F_{5/2}$

Table A4. Excerpt of line list for model used to match observations on 1994 October 11. The full table is available as Supporting Information.

λ (Å)	W_λ (Å)	Species	Transition (upper level – lower level)
3202.5	−4.0	Ti II	$3d^2$ (^{1}D) 4p $y^2F^o_{5/2}$ – $3d^2$ (^{1}D) 4s $a^2D_{3/2}$
3203.4	−2.7	Ti II	$3d^2$ (^{3}F) 4p $z^2F^o_{5/2}$ – $3d^2$ (^{3}F) 4s $a^4F_{3/2}$
3210.4	−4.8	Fe II	$3d^6$ (^{5}D) 4p $z^4D^o_{3/2}$ – $3d^7$ $a^4P_{1/2}$
3212.0	−2.3	Fe II	$3d^6$ (^{3}H) 4p z4$I^o_{9/2}$ – $3d^6$ (^{3}G) 4s $b^2G_{9/2}$
3213.3	−6.2	Fe II	$3d^6$ (^{5}D) 4p $z^4D^o_{5/2}$ – $3d^7$ $a^4P_{3/2}$
3214.8	−3.2	Ti II	$3d^2$ (^{3}F) 4p $z^2F^o_{7/2}$ – $3d^2$ (^{3}F) 4s $a^4F_{9/2}$
3216.9	−1.5	Ti II	$3d^2$ (^{1}D) 4p $y^2F^o_{7/2}$ – $3d^3$ $a^2G_{7/2}$
3217.1	−5.5	Ti II	$3d^2$ (^{3}F) 4p $z^4F^o_{9/2}$ – $3d^2$ (^{3}F) 4s $a^4F_{7/2}$
3218.3	−3.1	Ti II	$3d^2$ (^{1}G) 4p $y^2G^o_{7/2}$ – $3d^3$ $a^2H_{9/2}$
3222.8	−5.8	Ti II	$3d^2$ (^{3}F) 4p $z^4F^o_{7/2}$ – $3d^2$ (^{3}F) 4s $a^4F_{5/2}$

SUPPORTING INFORMATION

Additional Supporting Information may be found in the online version of this article:

Table A1. Line list for model used to match observations on 1994 September 1.
Table A2. Line list for model used to match observations on 1994 September 9.
Table A3. Line list for model used to match observations on 1994 October 1.
Table A4. Line list for model used to match observations on 1994 October 11.

Please note: Wiley-Blackwell are not responsible for the content or functionality of any supporting materials supplied by the authors. Any queries (other than missing material) should be directed to the corresponding author for the article.

This paper has been typeset from a TEX/LATEX file prepared by the author.